

University of
BRISTOL



**SOUTH WEST
NUCLEAR HUB**

Optimization of Pulsed Direct Current Plasma-Assisted
Chemical Vapour Deposition (PDC PA-CVD) and its
Use to Create Isotopically Pure Diamond for Radiation
Detection Applications

Edmund Smith

Course: MSc Nuclear Science and Engineering

Year: 2017

Supervisor: Professor Tom Scott

Words: 9219

Declaration

I declare that the work in this dissertation was carried out in accordance with the requirements of the University's Regulations and Code of Practice for Taught Programmes and that it has not been submitted for any other academic award. Except where indicated by specific reference in the text, this work is my own work. Work done in collaboration with, or with the assistance of others, is indicated as such. I have identified all material in this dissertation which is not my own work through appropriate referencing and acknowledgement. Where I have quoted or otherwise incorporated material which is the work of others, I have included the source in the references. Any views expressed in the dissertation, other than referenced material, are those of the author.

SIGNED: DATE:

Contents

Abstract.....	iv
Acknowledgments.....	v
Chapter 1: Introduction.....	1
1.1 Theory of diamond growth by chemical vapour deposition	3
1.2 Pulsed DC plasma-assisted CVD.....	6
1.3 Use of ¹³ C diamond in radiation detection.....	9
1.4 Project aims and objectives.....	12
Chapter 2: Experimental	13
2.1 Reactor design.....	13
2.2 Standard deposition method.....	16
2.3 Characterisation of diamond depositions	18
2.3.1 Scanning electron microscopy (SEM)	18
2.3.2 Raman spectroscopy	18
Chapter 3: Results and Discussion.....	19
3.1 Optimization of the PDR	19
3.1.1 Cleaning of the substrates and electrodes	19
3.1.2 Plasma stability	21
3.1.3 Cooling of the substrate and electrodes during deposition	24
3.2 Diamond growth and characterisation	26
Chapter 4: Conclusions and Future Research	41
4.1 Summary.....	41
4.2 Future work.....	42
References.....	42

Abstract

Isotopically pure ^{13}C diamond has good potential to be a superior material to silicon in radiation detection devices. In order to generate the high quality ^{13}C diamond films required for such devices, a PDC PA-CVD apparatus has been built, but still requires optimization to produce the desired diamond. By improving plasma stability and growth conditions, good quality diamond crystals have been grown, and with improvements to reproducibility, high quality diamond films should be easily generated.

Acknowledgments

I would like to thank Dr. Neil Fox for his suggestions and direction all through this project: without his insight, I wouldn't have made it far. Also, thanks to Dr. James Smith for his constant support and general helpfulness, teaching me the basics of using the PDR and the Raman kit, and providing a positive boost at times when the tiresome nature of the PDR was getting frustrating.

Thanks also to Prof. Paul May for his invaluable advice, Ian Bickerton for his help in using the DELPHI software, Alex Croot for his help with the Raman, and Ed Mahoney for his efforts in helping me obtain spectroscopic data and being very accommodating with not using his MWCVD reactor when I wanted to do depositions. Finally, thanks to Dominic Palubiski and Venkateswara Sodisetti, who made sure I had sufficient time to do the runs I wanted and generally made this project an enjoyable one.

Chapter 1: Introduction

Diamond has traditionally been prized for its scarcity, featuring significantly throughout history as a symbol of wealth [1]. However, diamond's other properties have made it a material of great interest for both scientists and engineers alike: diamond exhibits extreme mechanical hardness (*ca.* 90 GPa), high atomic density (10^{12} N m^{-2}), high thermal conductivity ($10^3 \text{ W m}^{-1} \text{ K}^{-1}$), modifiable electrical conductivity – ranging from a very good insulator ($10^{13} \Omega \text{ cm}$) to a semiconductor with a band gap of 5.5 eV – all while being resistant chemically, biologically and to radiation [2]. Diamond consists of tetrahedral sp^3 hybridised carbon in a 3D lattice, while the most common form of carbon – graphite – is more stable in its sp^2 hybridised layered form, shown in figure 1.1. Diamond's metastable nature, being slightly less thermodynamically stable than graphite and only being separated by a large activation barrier, has simultaneously caused its rarity, but also allowed for its existence, as diamond is unable to convert to graphite at mild conditions [3].

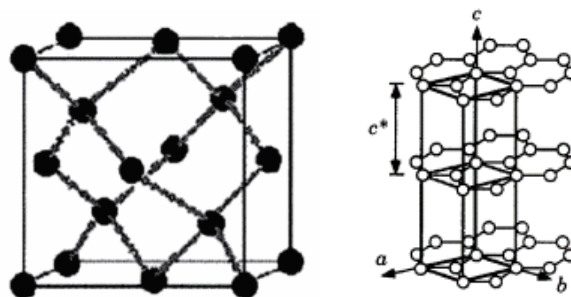


Figure 1.1: Structure of diamond (left) [4] and graphite (right) [5].

As such, early attempts to create diamond synthetically utilised temperatures of $3000 \text{ }^\circ\text{C}$ and pressures of 50,000 atm to mimic – and exceed – the conditions at which diamond forms in nature – called the high-pressure high-temperature (HPHT) technique [4,6]. However, the HPHT method was hindered by the limited size of single crystal diamonds that could be generated – ranging from nanometres to millimetres – and thus unable to fully utilise many of the extreme properties of diamond, so another method was required to allow growth of larger diamond films [7]. Hence, another method was developed which, rather than attempting to duplicate nature, produced diamond using a hydrocarbon gas as fuel at lower temperatures (from 700 to $1000 \text{ }^\circ\text{C}$) and much lower pressures (between 0.1 and 0.5 atm) [8]. Using plasma or filaments, the gas could be ionised into radicals which would deposit onto a substrate seeded with nanodiamond, with the addition of hydrogen gas to etch away any graphite which was co-deposited [9]; this process was called chemical vapour deposition (CVD) [10].

Using CVD processes, diamond growth could be adjusted, allowing control over the purity, size and shape of the produced diamond while maintaining the favourable properties of natural diamond, while depositing on a range of different substrate materials [11]. CVD processes also have the potential to further modify the properties of the diamond through the use of dopant gases during growth, hence making CVD more versatile than HPHT in terms of control over the diamond generated [12].

As such, CVD diamond has found use in a wide range of applications: some in improving existing technology and some in evolving new technology [2]. Due to its extreme thermal conductivity and low thermal expansion, diamond is being grown to act as a heat spreader in recent research on GaN for use in high-power communication technology, with the diamond extending the lifespan and increasing performance of the GaN [13]. Another application is in the use of diamond for neural implants, with diamond's excellent biocompatibility encouraging the growth of stem cells onto the surface, which allows for a connection between neurons and computers, especially when utilising boron-doping to yield conductive diamond [14].

One potential application is in radiation detection: diamond's radiation hardness, low intrinsic noise and high collection efficiency suggest that diamond would be a superior material for use in solid state radiation detection devices over commonly-used silicon [15]. Such devices have existed since the 1940s [16], but were costly and inefficient due to the lack of availability of high quality diamond films, such as those which can now be grown by CVD processes. Hence, there has only recently been increased focus on diamond radiation detection devices as diamond films are readily available. Isotopically pure ^{13}C offers new opportunities to improve diamond-based radiation detection devices due to the enhancement of some of diamond's properties, such as a modified band-gap [17], improved thermal conductivity [18] and increased structural strength [19], but there is little research on ^{13}C diamond compared to natural (99% ^{12}C , 1% ^{13}C) diamond.

The research undertaken for this project utilized a newly built pulsed direct current plasma-assisted CVD (PDC PA-CVD) reactor at the University of Bristol, and mostly concerned the optimization of this reactor towards growing high quality diamond films, with the aim of enabling the reactor to grow diamond for use in radiation detection devices. The method of PDC PA-CVD used, discussed herein, has the potential to grow suitable diamond films, with the ability to generate isotopically pure ^{13}C diamond in the longer term.

1.1 Theory of diamond growth by chemical vapour deposition

Chemical vapour deposition (CVD) is the process of material deposition onto a substrate using an activated gas mixture. This technique can be used to grow a large range of materials, such as transition metals, C (nanotubes, graphene and diamond), B, Si and many silicon- and carbon-containing compounds, with high quality being achieved at the cost of a low growth rate; hence, CVD techniques are usually used to generate films, rather than significant bulk [20].

For diamond CVD, the grain sizes can vary from ultrananocrystalline to microcrystalline, being either mono- or poly-crystalline in form: these properties may be modified by altering the CVD technique used and offers a wide variety of applications. Diamond CVD comprises of several interconnected processes, as shown in figure 1.2.

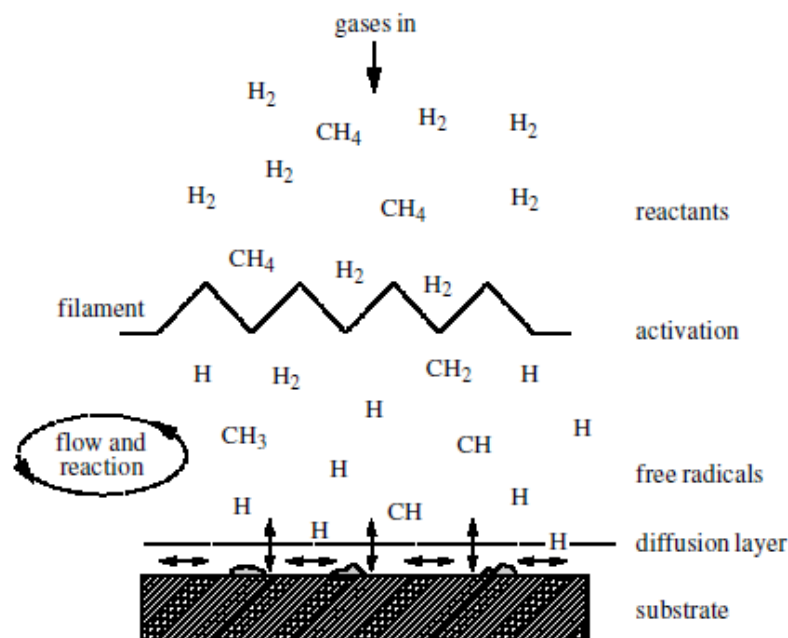


Figure 1.2: Schematic of chemical and physical processes involved in diamond CVD, from [21].

Process gases – H_2 and CH_4 – enter the chamber and diffuse towards the substrate. As they pass through the activation region (*e.g.* a hot filament, microwave plasma or electrical discharge), the gases are ionized, liberating electrons and reactive radicals, and increases the gas temperature to *ca.* 2000 K. These fragments continue to mix and react with each other until they reach the substrate surface, where they may adsorb to the surface and, if all the conditions are suitable, grow diamond.

Atomic hydrogen, H, generated either by thermal decomposition of H₂ in hot filament systems or by electron impact dissociation of H₂ in plasma systems, drives the CVD process by:

- i. Termination of “dangling bonds” on the deposition surface, avoiding reconstruction of the sp³ surface to sp² graphite.
- ii. Etching sp² graphitic carbon much faster than sp³ diamond-like carbon, thus removing graphite impurities during growth.
- iii. Breaking up any long-chain hydrocarbons into smaller pieces, which are better for uniform diamond deposition.
- iv. Reacting with neutral species (*i.e.* CH₄) to create reactive radicals (CH₃), which can deposit onto surface sites.

A simplified mechanism for deposition at the surface can be considered as site activation by H followed by the addition of CH₃ at the activated site, and the subsequent exothermic formation of a carbon-carbon bond to generate another new site above that which has been deposited, as shown in figure 1.3. Thus, diamond deposition is a stepwise addition of carbon atoms onto the diamond surface, which is catalysed by the excess H [21]. This mechanism, while sufficient as a simple model, does not account for the gas phase chemistry, the reactor used or the orientation of the diamond lattice, with significant differences in growth between the square (100) and triangular (111) surfaces, particularly with respect to optimal temperatures and gas conditions.

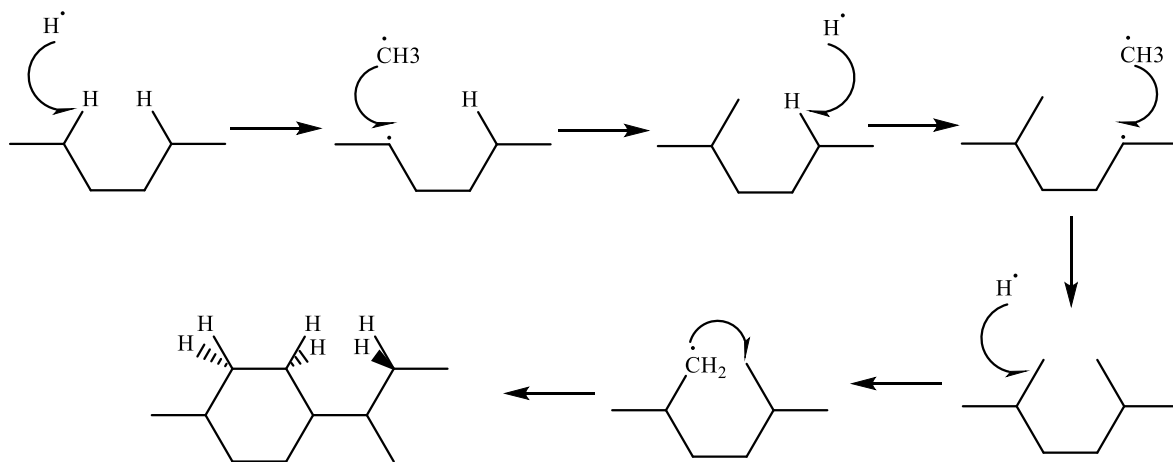


Figure 1.3: Mechanism of reactions of radicals at the diamond surface, leading to addition of CH₃ and diamond growth, reproduced from [22].

As shown in figure 1.2, activation is required in order to ionize the precursor gases; CVD reactors are defined by the means in which they activate the gases. Most methods utilize substrate temperatures above 700 °C, and typically have gas mixtures of 1–5% CH₄ in H₂.

Hot filament CVD (HFCVD) uses gases flowing at a constant rate (usual total flow rates of *ca.* 200 sccm), with a maintained pressure of 20-30 Torr and a substrate heater to keep the substrate of Si or Mo at 700-900 °C. Above the substrates is a filament which is heated electrically to *ca.* 2200 °C, which thermally ionizes the process gases. W and Ta are commonly used for the filament, as they can withstand the conditions, reacting sufficiently slowly to form metal carbide that long duration depositions are achievable; Re is an alternative offering more resistance to carburization, hence a longer lifespan but at a significantly higher material cost. HFCVD is one of the most common techniques, due to the simple design (shown in figure 1.4a) and operation along with reasonable quality polycrystalline diamond, but is hindered by slow growth rates (1–10 μm h⁻¹) when compared to other methods. However, due to the use of a metal filament, this technique is poorly suited to addition of dopant gases (as they will significantly reduce the filament’s lifespan), and the diamond is not of sufficient quality for many electronic applications [21].

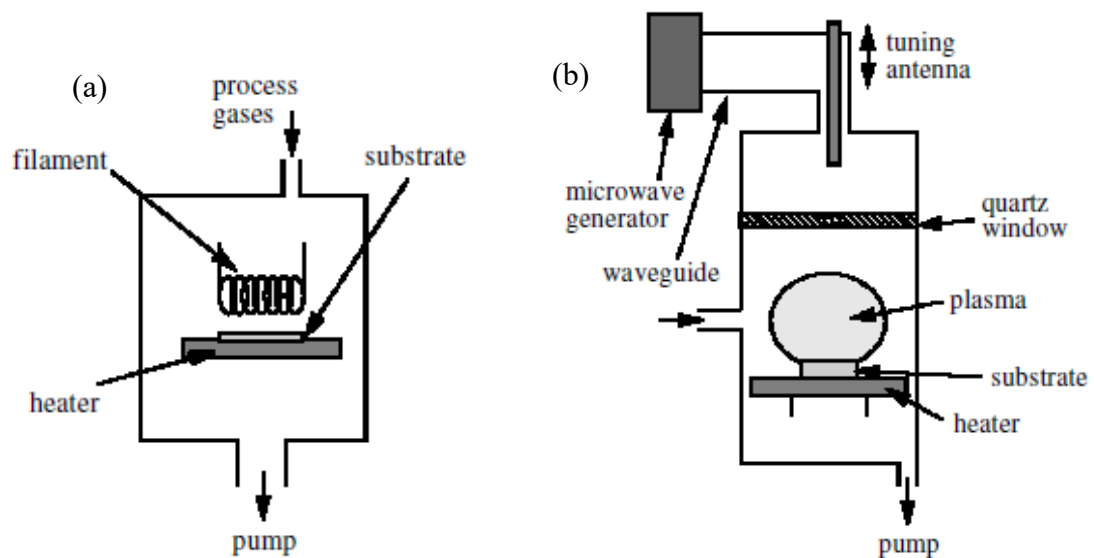


Figure 1.4: Examples of the most common CVD reactors, from [22].

(a) Hot filament, (b) “ASTEX-type” microwave plasma reactor.

Microwave plasma CVD (MWCVD) uses similar conditions to HFCVD, but with activation from microwave power coupled into the chamber *via* a quartz window to yield a discharge, which provides gas phase electrons with sufficient energy to ionize the reactant gases and heat both the gas and substrate to adequate temperatures, shown in figure 1.4b. With the capacity to deposit at a high rate of 10-30 $\mu\text{m h}^{-1}$ over substrates up to 10 cm in diameter due to the higher power input attainable, MWCVD is the most commonly used CVD technique, especially with industrial diamond manufacturers [23]. Microwave systems are also able to utilise a wide range of gases, including oxides, chlorides and fluorides, which hot filament systems cannot, allowing for diverse doping of the diamond to suit a range of applications: for example, the addition of N_2 gas reduces crystal size from microcrystalline to nanocrystalline. The high purity of diamond generated makes MWCVD the preferred system for electronic applications [24].

Plasma jets use high gas flow rates and high-power electrical arcs to ionize the reactant gases, which then deposit onto the substrate. This method leads to very rapid growth (usually about 100 $\mu\text{m h}^{-1}$, highest reported 900 $\mu\text{m h}^{-1}$ [25]) but at the cost of deposition area (often *ca.* 1 cm^2), which, along with issues due to thermal shock, has rendered it a rarely used technique. A similar method using acetylene and oxygen gases with a welding torch was briefly used, but suffered similar hindrances as plasma jets [26].

The final method to be mentioned is pulsed direct current plasma-assisted CVD (PDC PA-CVD), which is the technique chosen for the research this report focusses on. As such, this technique will be looked at in more detail.

1.2 Pulsed DC plasma-assisted CVD

Direct current plasma-assisted CVD uses two parallel electrodes with a DC voltage applied to the cathode and the anode grounded, which generates a plasma of the H_2 and CH_4 gases, shown in figure 1.5. At lower voltages, the gas is insulating; however, as voltage increases, gas phase electrons are liberated and accelerated towards the anode, resulting in ionization of the reactant gases. The positively charged ions generated are themselves accelerated towards the cathode, freeing electrons from the electrode, causing secondary electron emission. The resultant electron avalanche, often termed the Townsend discharge, is followed by complex gas breakdown mechanisms to form the desired reactive radicals, “activating” the plasma and providing the suitable conditions for diamond deposition to begin.

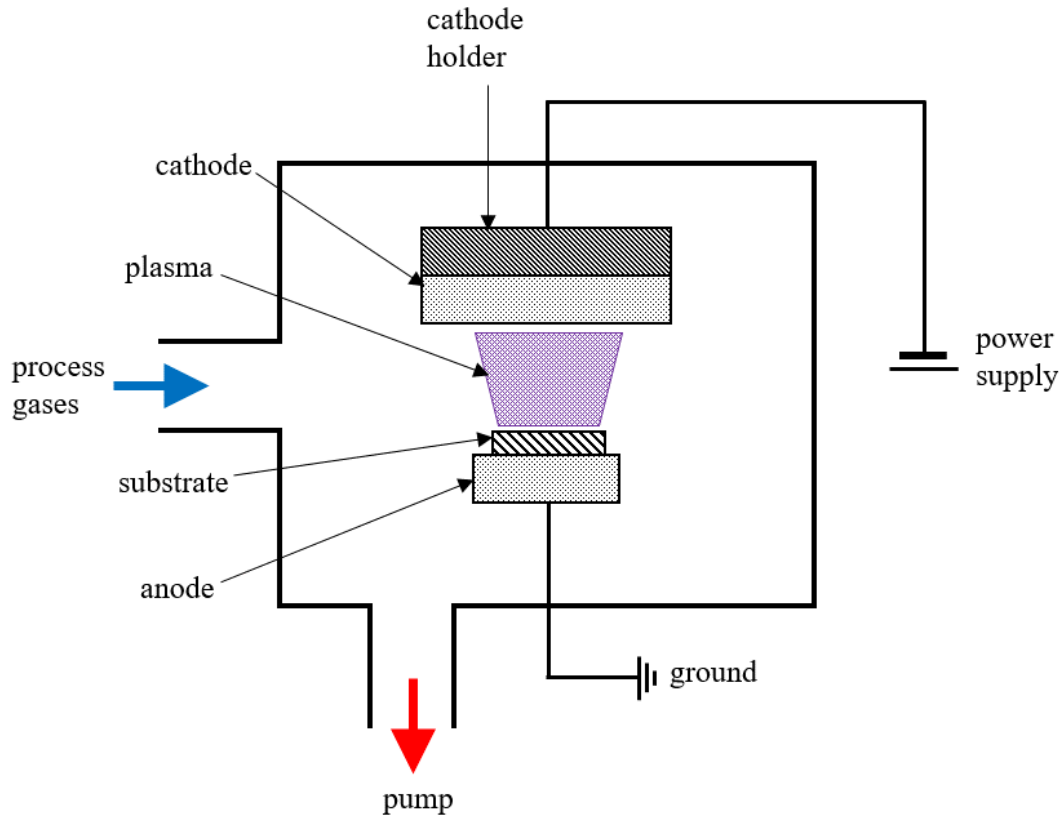


Figure 1.5: Schematic diagram of a DC plasma-assisted reactor.

The potential field required for this electron avalanche is determined by the specific breakdown voltage, V_b , dependent on the pressure, p , and electrode separation, d , which can be determined by Paschen's law (equation 1) [27]:

$$V_b = \frac{Bpd}{\ln(Apd) - \ln\left[\ln\left(1 + \frac{1}{\gamma_{se}}\right)\right]} \quad (1)$$

where: A and B are constants for a given gas
 γ_{se} is the secondary electron emission

DC plasmas can be classified by their current and voltage characteristics, with different types of plasma exhibiting different properties, shown in figure 1.6. Until V_b is reached, there is dark discharge, but increased power only leads to increased voltage (from B to C), with the plasma acting as an insulator. With sufficient potential V_b (E), a glow discharge forms, which is the region where DC CVD reactors usually operate. For a normal glow (F to G), increased current yields an increased cathode current density; abnormal glow occurs when the cathode current

density (the cathode spot) cannot increase, so increased current results in an increased potential field (G to H). In order to achieve the required gas and electron temperatures for diamond deposition, abnormal glow is required. However, if the current becomes too high, then arcing may occur, reducing the voltage as current is able to flow more easily, which causes a drop in the gas temperature and ends deposition.

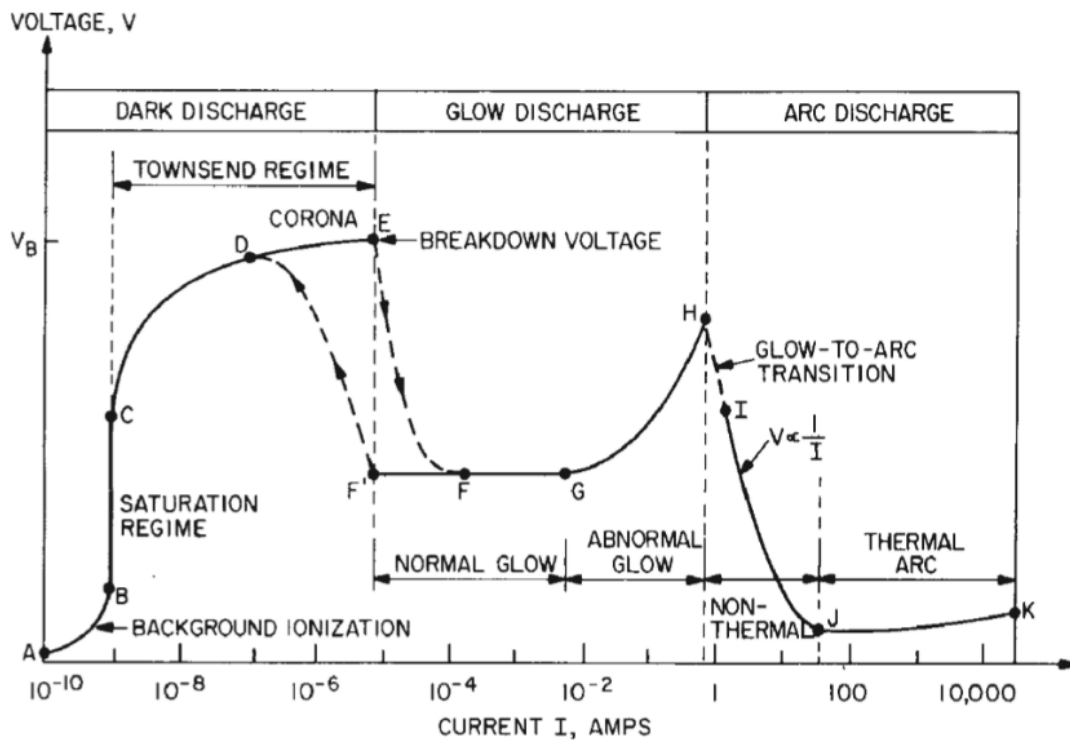


Figure 1.6: Regions of the classical DC electrical discharge, from [28].

DC plasma-assisted CVD was seen as a promising technique after initial successes, especially with high growth rates (often $10\text{-}50 \mu\text{m h}^{-1}$ [29,30], sometimes over $100 \mu\text{m h}^{-1}$ [31]) and the capacity to grow over large substrates (10 cm diameter wafers in 2001 [32] and 2003 [30], 20 cm diameter wafers in 2010 [33]) without surface treatment [34]. However, DC plasma-assisted CVD failed to gain the popularity of HFCVD and MWCVD techniques, and as such, there is much less known about them: this can be attributed to the difficulties faced by many groups in achieving and maintaining stable plasmas [35,36,37,38]. The technique of pulsing the direct current – hence, pulsed direct current plasma-assisted CVD – has been shown to yield more stable plasma and reduce the likelihood of arcing, allowing for the use of high powers to maintain good growth rates over larger areas [29,39,40].

However, given the long-term desire to attempt growth of isotopically pure ^{13}C diamond for radiation detection devices, PDC PA-CVD becomes the most suitable growth method. This is mainly due to the open choice of substrate and the lack of surface treatment required for growth. Both Mo [29,33] and Si [34] have been grown on successfully, with no noticeable differences when using polished or non-polished surfaces and no seeding with nanodiamond required for initial nucleation, unlike hot filament and microwave processes. This allows for more flexibility in substrates used, so, for example, diamond can be grown directly onto a surface which can also act as an anode for radiation detection, so long as the material is able to withstand the conditions within the reactor. For pure ^{13}C diamond growth, seeding with nanodiamond would be expensive due to the low availability of ^{13}C diamond, so other CVD techniques would become very costly or natural ^{12}C nanodiamond would have to be used, introducing an impurity: PDC PA-CVD is not hindered with the requirement of seeding, making this technique the best option for the longer-term objective of ^{13}C diamond growth.

1.3 Use of ^{13}C diamond in radiation detection

Diamond has been used in radiation detection since the 1940s [16], but failed to compete against silicon-based devices due to the poor quality and high expense of diamond at the time. However, with the availability of cheap, electronic quality CVD diamond with a modifiable band gap, there is new potential for diamond radiation detection devices to replace silicon-based devices [41].

Solid state detectors operate by detecting the energy left by interactions between the incident particle and the atomic electrons in the material. For solids of an atomic lattice, electrons are excited from the valence to the conduction band when the particle transfers sufficient energy: a process called electron-hole generation. Detection is based on the Bethe formula [42] and Landau distribution [43], determining the energy deposited into the material for a traversing particle and for a particle stopped by the material respectively.

In order to maximize the signal-to-noise ratio, detectors are made of thin layers of material (usually *ca.* 300 μm), with electrodes either side to apply a bias voltage, to drain the signal. Solid state detectors are often referred to as “semiconductor detectors” as they are usually made of semiconducting Si, with a pn-junction being utilised to remove the intrinsic charge from the bulk of silicon and to assist in detection of a signal.

However, diamond is superior to silicon in some respects: diamond's lower atomic number means that particles are less likely to be absorbed or scattered, allowing for full traversal of the detector, and hence a more resolved particle energy measurement; diamond's band gap of 5.5 eV [44] results in a much lower intrinsic carrier density n_i than Si with a band gap of 1.11 eV [45], as shown by equation 2 [46]:

$$n_i^2 = N_C N_V e^{-\frac{E_g}{kT}} \quad (2)$$

where: N_C and N_V are weights of conduction and valence bands

E_g is the band gap

k the Boltzmann constant

T the absolute temperature

Lower intrinsic carrier density means that more energy must be transferred for the excitation of an electron into the conduction band, making the material better suited for detection of high-energy particles: for diamond, the intrinsic carrier density is so low that the pn-junction is not required, as the polarity of the field is effectively irrelevant. Diamond also has a low dielectric constant, which reduces the capacitance of detection devices, allowing for simple two-terminal metal-insulator-metal devices with a low noise [47], making diamond-based devices simpler than most other solid state devices. Coupled with this, diamond has a high carrier mobility, resulting in very fast signal collection times – 1 ns in a 500 μm thick detector, with the capacity to count heavy ion rates above $10^8 \text{ cm}^{-2} \text{ s}^{-1}$ [46].

Polycrystalline diamond has a low charge collection efficiency (*ca.* 30%), due to the short mean free paths generated by the grain boundaries. However, modern CVD techniques can produce large enough monocrystalline diamond for use as detectors, with efficiencies of 97% reported, alongside excellent energy resolution [48].

Diamond's large band gap, large displacement energy and high thermal conductivity result in extreme radiation tolerance, with very low leakage currents and the ability to be used without cooling, making diamond devices particularly attractive for high energy, high flux radiation applications [49,50,51]: one such application is in fusion reactors, such as JET and ITER. CVD diamonds have been used for high energy neutron (14 MeV) detection in the JET fusion reactor during the 2005-2007 experimental campaigns [52,53,54], shown in figure 1.7. Due to the

ability of the single crystal diamond being able to discriminate between the total and high energy neutrons, these detectors are the first to simultaneously measure both the total and 14 MeV neutron yields with good reliability and stability [53]. The HPHT diamond substrate was not removed, as doing so is expensive and often damaged the high-quality diamond film for detection; the ${}^6\text{Li}$ in the LiF reacts readily with thermal neutrons to generate α particles, which are in turn detected by the CVD diamond below, allowing for the simultaneous detection of thermal and 14 MeV neutrons.

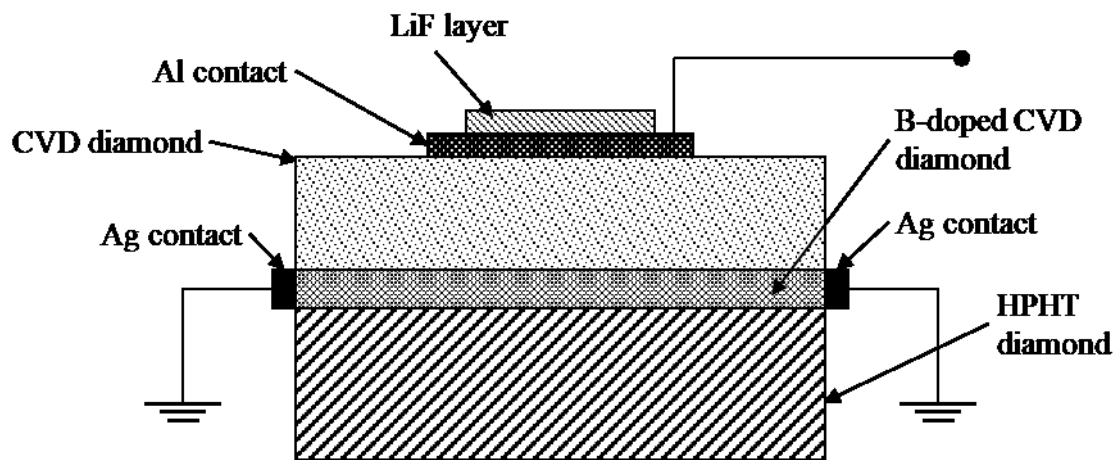


Figure 1.7: Scheme of diamond detector used at JET, from bottom to top: HPHT diamond substrate, boron-doped CVD layer, high-purity single crystal CVD diamond, aluminium contact, ${}^6\text{LiF}$ layer, reproduced from [53].

Isotopically pure ${}^{13}\text{C}$ diamond may offer several potential advantages over ${}^{12}\text{C}$ diamond in radiation detection applications. ${}^{13}\text{C}$ diamond has shorter bonds, resulting in increased structural strength [19], which should enhance the diamond's radiation hardness, increasing the lifespan of a detection device. Higher isotopic purity has been shown to further improve the already excellent thermal conductivity of diamond [18], while ${}^{13}\text{C}$ diamond slightly increases the band gap between the valence and conduction bands. This shift would improve resolution of detected particle energy, as would the improved attenuation from the increased electron density within the more compacted diamond lattice. ${}^{13}\text{C}$ is not ideal for usage in high energy neutron environments, as ${}^{13}\text{C}$ has a higher neutron capture cross section than ${}^{12}\text{C}$ for neutrons in the 10^4 - 10^7 eV energy range [55], yielding radioactive ${}^{14}\text{C}$ which is undesirable, both for the potential safety hazard it presents, but also that its β decay will be detected and leave ${}^{14}\text{N}$ as a defect in the diamond lattice, reducing detection efficiency.

However, there is a general lack in information regarding ^{13}C diamond, due to the challenges regarding nanodiamond seeding faced with CVD methods other than DC PA-CVD, so any synthesis and subsequent investigation into the properties of isotopically pure ^{13}C diamond would be a worthwhile venture.

1.4 Project aims and objectives

The primary aim of the work undertaken was to achieve consistent and reproducible diamond growth using the PDC PA-CVD system, with the longer-term aims of producing high quality diamond thin films suitable for use in radiation detection devices and then utilizing the potential of the apparatus for production of isotopically pure ^{13}C diamond for radiation detection applications.

The primary aim was to be approached in several ways: initially, work would focus on obtaining stable and uniform DC plasmas, and then move onto trying to achieve optimal growth conditions, both on the substrate and in the plasma. Following this, growth attempts would be aimed at maintaining consistent diamond production from run to run.

This approach was chosen following the limited success of others trying to optimize the apparatus: previous attempts have focussed on using Taguchi optimization techniques [56], which tries to avoid a “trial and error” approach in favour of a more efficient optimization of many parameters simultaneously. However, given the realization that the variables are difficult to isolate with the PDC PA-CVD apparatus – changing one variable automatically changes several others and “identical” consecutive runs result in very different outcomes – the choice was made to focus on achieving one outcome at a time, and use a more stochastic attitude to experimental conditions to find a set of variables that can consistently produce that outcome.

Hence, this research is carried out with the objectives of improving plasma stability, achieving optimal diamond growth conditions and growing high quality diamond, either as a film or as crystals, overall further aiding in the optimization of the PDC PA-CVD apparatus towards being able to grow consistent, high quality diamond thin films.

Chapter 2: Experimental

2.1 Reactor design

The Pulsed DC Deposition Reactor, PDR, at the University of Bristol was constructed in 2015, with the first growth runs taking place in early 2016 [57] and the first diamond grown later that year [58]. The reactor is comprised of a water-cooled steel bell jar containing DC plasma deposition equipment, with a borosilicate window which allows safe viewing of the plasma and the substrate, shown in figure 2.1.

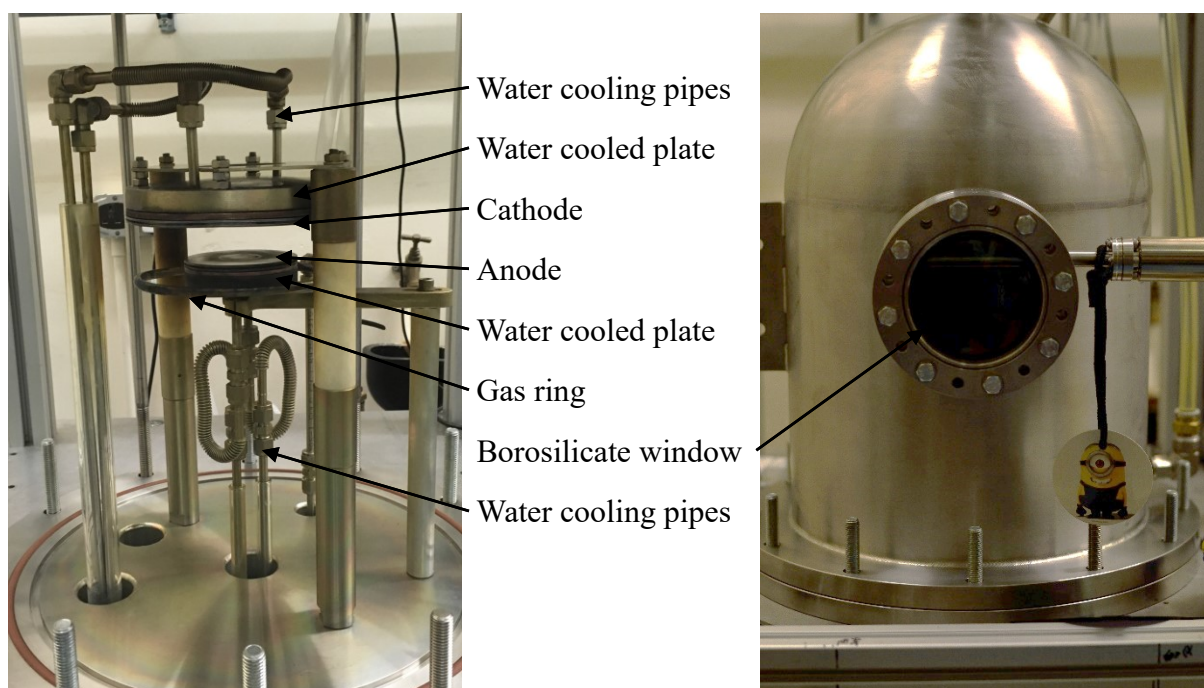


Figure 2.1: left: Photograph of the interior of the PDR, showing the DC plasma deposition equipment, from [58], with the components labelled; right: Photograph of the outside of the steel bell jar of the PDR.

The DC plasma deposition apparatus consists of two fixed parallel electrodes, made of Mo and 4 mm thick. The larger cathode (152 mm diameter) is connected to the power supply (Advanced Energy Pinnacle Plus Pulsed-DC [59]) while the anode (76 mm diameter) is grounded, onto which the substrate for growth is placed. A wire ring spacer (Ta or W, 0.25-1 mm diameter) is positioned between the Mo electrodes and a Cu plate (4 mm thick, diameter equal to that of the electrode), which in turn are attached to the water-cooled steel plates (13 mm thick), all which combine to allow the optimum temperature for each electrode to be

reached. The water cooling system circulates deionised water into the steel plates at inlet temperatures of 9-13 °C, through Cu pipes (inside the pressure vessel) and PFA pipes [60] (outside of the pressure vessel, rated for 70 °C), and the flow is shared with a MWCVD reactor which is also in the laboratory – details of the effect of this on the PDR can be found in Chapter 3.1.3. The steel bell jar (610 mm high, 305 mm internal diameter and 356 mm external diameter) is also water-cooled by the same system, and the distribution of water flow between the cooling for the electrodes and the cooling for the bell jar can be adjusted. The borosilicate glass window, shown in figure 8 (alkali borosilicate 7056; Kodial [61], 95 mm diameter) allows high transmission of optical and near infrared-wavelength light (200 nm to 3 μm [61]) and absorbs the UV radiation emitted from the plasma, allowing optical emission spectroscopy, OES, to be used to examine plasma composition safely. Within the ceramic of the cathode mounting are Cu feedthroughs, which inlet the power to the cathode while ensuring isolation from the grounded components nearby.

The power supply [59] converts 3-phase AC into the desired pulsed DC: it has the capacity to provide a maximum of 10 kW, 660 V and 30.8 A (with one of the three dependent on the limitations of the other two according to $P = VI$ at a given time). The output is usually manually controlled by power (with the power supply determining the other two), but has voltage and current regulation modes available, which were tested but determined to be less practical than power regulation mode – see Chapter 3.2 for experimental results. The power supply has built-in arc suppression, where it periodically reverses electrode voltage to reduce the build-up of charges and hence reduce the likelihood of arcing; it is also able to respond quickly to minimize arc damage, suppressing micro-arcs within 5 μs and hard arcs within 200 μs, although some arcing did still occur experimentally. Frequency of the DC pulses can also be manipulated from 0-150 kHz. Another useful function of the power supply is “ignition capability”, in which the supply can provide voltages up to 1500 V for a brief period to aid in striking the plasma. [59]

Mass flow controllers (Bürkert Type 8715 MFC for Gases [62]) utilizing a thermal capillary sensor are used to inlet the process gases into the chamber *via* the grounded gas ring, which currently has a similar diameter to the cathode, sits just below the anode and directs gases into the space between the two electrodes, shown in figure 2.1. The pressure inside the chamber is determined using a 10 Torr manometer (Baratron, MKS [63]) at low pressures, such as during evacuation of the chamber or when striking the plasma, and a 1000 Torr manometer [63] at the

higher pressures used for growth. The pressure can be controlled by a butterfly valve on the exhaust line, with a rotary vane pump (Edwards RV12 [64]) continually evacuating the line.

The pressure within the chamber and the gas flow rates into the chamber are controlled using in-house designed DELPHI software, which also monitors the temperature of the PFA pipes in the water cooling outlet from the electrodes, while the power supply is currently independently controlled. The limitations of the current equipment are listed in table 2.1.

Table 2.1: Equipment limitations of the PDR.

	Minimum	Maximum
Pressure / Torr	0.014 ^a	760 ^b
H ₂ flow / sccm	0	500
CH ₄ flow ^c / sccm	0	50
Power / kW	0	10
Voltage / V	0	660
Current / A	0	30.8
Electrode separation / mm	<i>ca.</i> 1	50
Water cooling input / °C	9	13
Water cooling output ^d / °C	12	70

Mo and W disks were manufactured from larger pieces (assorted 3 mm, 4 mm and 5 mm thicknesses, 30 mm diameter, <1 mΩ resistance) for use as substrates. Mo and W were chosen for their high melting points, low reactivity with the process gases, similar thermal expansion coefficients to diamond and ability to form a carbide layer while at temperatures of *ca.* 1000 °C [65]. As growth without a seeding layer is achievable with PDC PA-CVD, and hence the reason for using the method to grow isotopically pure samples, the substrates were not seeded with nanodiamond unless explicitly stated.

All diamond deposition reported herein uses the PDR, with H₂ (99.999% purity, Air Liquide) and “natural” CH₄ (99% ¹²C and 1% ¹³C, 99.995% purity, Air Liquide) used as feedstock gases.

^a Lowest measured base pressure. This pressure is lower than was achieved before and may be the result of new cleaning methods being used. See Chapter 3.1 for more information.

^b Atmospheric pressure is 760 Torr – torr is the preferred unit of pressure for CVD reactors.

^c The current setup uses the same MFC for CH₄, ¹³CH₄ and N₂ feedstocks, so for CH₄ only is given.

^d This are the minimum and maximum temperatures read by thermocouples attached to the PFA pipes without the pipes bursting.

2.2 Standard deposition method

A substrate was placed on a Ta or W wire ring spacer in the centre of the surface of the Mo anode, the bell jar lowered and the chamber evacuated to <20 mTorr. Once a sufficient pressure was achieved, H₂ gas was inlet at 500 sccm and the pressure allowed to equilibrate to *ca.* 1.8 Torr for a few minutes, allowing for residual air to be diluted to near-zero quantities. The power supply was then turned on, striking the plasma at 50 W (aided by the “ignition capacity” of the power supply) at 100 kHz. The pressure was slowly increased to 100 Torr (at a rate of 0.3 Torr s⁻¹) using the DELPHI software, with power manually increased simultaneously – usually power of 1 kW at 40 Torr and 2 kW at 100 Torr. During this time, the pulse frequency was often varied from 100 kHz to 10 kHz to assist in forming a stable, uniform plasma over the entire surface of the substrate, but was returned to 100 kHz before increasing the pressure above 100 Torr due to increasing instability. From there, the pressure was further increased to 175-200 Torr – growth conditions from literature sources [29,30,33,66,67], shown in figure 2.2 – and the power increased in order to achieve the desired field strength.

Table 2.2: Typical desired growth conditions for diamond deposition, from [29,30,33,66,67], and approximate values used experimentally.

	Minimum	Maximum	Used
Pressure / Torr	100	200	175-200
H ₂ concentration / %vol	93	98	96
CH ₄ concentration / %vol	2	7	4
Gas flow / sccm	200	500	520
Current / A	4.5	89 ^e	6-10
Voltage / V	320	850	500-650
Electrode separation / cm	0.5	2.5	2.0
Field strength / V cm ⁻¹	320	900	250-325
Substrate temperature / °C	750	1300	900-1200 ^f
Cathode temperature / °C	750	1000	800-1100 ^g

^e This current was used for growing 8 inch (20 cm) wafers [33], so is significantly higher than desirable for growth across a 3 cm substrate.

^f This temperature was difficult to measure to any precision – see Chapter 3.1.3.

^g This temperature was also difficult to measure – again, see Chapter 3.1.3.

Initially, CH₄ was only added when the pressure had reached 175-200 Torr, but during investigation of plasma stability, it was decided that CH₄ would be added at 100 Torr to yield a more stable plasma, discussed further in Chapter 3.1.2. Once deposition conditions were met, the voltage and current were monitored and, where appropriate, the power was increased in order to maintain the desired field strength.

At the end of deposition, due to loss of plasma stability, inability to maintain a sufficient potential field strength without damaging the water cooling apparatus, or sufficient time having passed, the power supply was switched off, the flow of CH₄ stopped and the butterfly valve opened. The H₂ gas flow was stopped after a few minutes had passed, to ensure hydrogen termination of deposited diamond and to aid in cooling, and the PDR left to cool and reach base pressure, after which the substrate was removed for analysis.

During preliminary test runs, mimicking runs performed by those attempting optimization on the PDR previously [57,58], it was quickly realised that three main areas in the operation of the PDR needed improvement: cleaning processes, plasma stability, and cooling. As such, these became the main points of focus in the optimization work being carried out, as discussed in Chapter 3.1. A repeating iterative approach was taken, using the information gained by previous runs to determine what conditions would be attempted in the next runs; diamond samples generated during the deposition runs were analysed, providing further information on the effect of changing the variables. The resultant diamond produced is discussed in Chapter 3.2.

Most of the depositions were done working alongside Dominic Palubiski and/or Venkateswara Sodisetti, and many of the ideas for runs were discussed with them. However, every deposition reported herein was performed by the author, and all SEM images, Raman spectra and photographs were taken by the author unless specified otherwise.

2.3 Characterisation of diamond depositions

Following the deposition runs, it was important that samples were appropriately analysed and characterised in order to determine the properties of any material grown. Given the generally very short growth runs, either a very thin film of diamond from nanocrystalline nucleation or larger independent diamond crystals were expected to be produced.

2.3.1 Scanning electron microscopy (SEM)

Scanning electron microscopy is one of the main methods in characterisation of CVD diamond, utilizing a focussed beam of electrons and monitoring their scattering, offering a non-destructive way to assess the size and quality of the diamond at the μm -scale. Images were taken using a Jeol JSM-IT300LV Versatile Research SEM at the Chemical Imaging Facility and a Zeiss Evo MA10 LaB₆ SEM at the Interface Analysis Centre, both situated within the University of Bristol, and used to assess the size of nucleated crystals and the overall uniformity of coverage across the substrate, along with a qualitative assessment of the quality.

2.3.2 Raman spectroscopy

Raman spectroscopy monitors the change in vibrational frequency of inelastic scattered light upon interaction with molecules. The shift in frequency allows elucidation of the vibrational modes and hence the composition of a material [68]. Single crystal diamond exhibits a characteristic sharp single peak at 1332 cm^{-1} when exposed to the light of a green argon ion laser (wavelength 514 nm), allowing for easy identification [69]. Diamond grown by CVD processes are usually a combination of nano- and micro-crystalline diamond, with some graphitic and amorphous carbon on the grain boundaries, resulting in a more complex spectrum: the sp^3 hybridised diamond peak at 1332 cm^{-1} and the sp^2 hybridised “disordered graphite” and graphite peaks, D and G, at 1350 cm^{-1} and 1580 cm^{-1} respectively [70]. Hence, the relative intensities of the diamond and G peaks are often used as a basic measure of diamond purity [71].

Using a Renishaw 2000 Laser Raman Spectrometer with a green argon ion laser of 514 nm, samples generated by the PDR were analysed, providing a quantitative measure of the quality and purity of the generated diamond. It is worth noting that when using a Raman wavelength of 514 nm, sp^2 carbon is detected more readily and hence shows a disproportionate peak size compared to sp^3 carbon.

Chapter 3: Results and Discussion

3.1 Optimization of the PDR

Overall, many issues were encountered experimentally. As mentioned in Chapter 2, deposition time for a growth run was often limited by plasma instability or by issues achieving and maintaining the required field strength for deposition to occur. During deposition, the cathode and substrate would become more resistive due to the accumulation of carbon on their surfaces and, in an effort to offset the effect of this on the plasma, the power supply would automatically increase the current, resulting in a decrease in the voltage to maintain the manually-input power. To compensate for this and maintain a sufficient field strength for growth, the power input would be increased, but this also increased the heat having to be removed by the water cooling, with the water cooling system imposing limitations on the power that could be used.

However, this issue was initially overshadowed by the challenges of getting the plasma to consistently form on the substrate – something that was clearly affected by the carbon deposition on the cathode, as uniform plasma became increasingly difficult to obtain after each of the preliminary test runs – resulting in the work on cleaning methods.

3.1.1 Cleaning of the substrates and electrodes

Establishing a repeatable and effective cleaning procedure for the electrodes and the substrates was very important. The carbon-based deposits on the cathode affected the shape of the plasma, and hence its stability, resulting in the plasma being less likely to form across the substrate, preferring a less resistive position to the side of the substrate, increasing the likelihood of arcing. Also, given the limited number of substrates available, reuse of them was required, so the cleaning method would also have to be able to clean the substrates of any deposits on them. Sandpaper quickly proved inefficient and the polishing apparatus available was not able to deal with the hardness of Mo, W or the C-based deposits. The only previously useful method of removing these deposits was by milling, but this took a lot of time and would require regular replacement of components due to wear, especially if being performed on a weekly basis.

As such, an easy but effective cleaning method utilising the potential for etching at temperatures within the PDR was investigated.

Initially, attempts to etch the carburization used plasmas containing H₂ (96%) and N₂ (4%), utilizing the etching abilities of atomic hydrogen and atomic nitrogen [72], at 150 Torr and 3.5 kW. In order to encourage etching of the substrates, higher temperatures were desired, so an additional substrate and wire ring spacer were placed between the substrate to be etched and the anode below. This yielded some etching, but, even after a cumulative duration of 2 hours over 3 runs, substantial deposits remained on both the substrate and the cathode. Subsequent attempts used pressures of up to 200 Torr and N₂ flow rates of 0-50 sccm (0%-9%), with no significant etching achieved: the highest etching rate measured was *ca.* 10 μm h⁻¹.

Having determined that this was not effective, etching was attempted with an additional substrate acting as a spacer (with a “tower” of three substrates on the anode, each separated by a wire spacer ring) at 200 Torr and 3 kW in a pure H₂ plasma, shown in figure 3.1. This plasma proved to be very effective, with the cathode being almost completely clean after 1 hour, and the substrate looking as though it was new.



Figure 3.1: H₂ “cleaning plasma” – 200 Torr, 3 kW, with 3 substrates each separated by a wire spacer ring. The lowest substrate, the anode and plasma are difficult to see due to the brightness of the top substrate.

With this “cleaning plasma” being used frequently, experiments run on the PDR became more consistent, given the capacity to restore the equipment to a set standard. Since then, it has been installed as a general practice to ensure the PDR is cleaned after every 2-3 growth runs.

3.1.2 Plasma stability

In order to achieve reproducible diamond deposition, the plasma generated by the PDR must be itself reproducible and stable, with uniformity across the substrate ensuring even deposition and consistent quality diamond films. The addition of CH_4 affected the stability of the plasma so the optimal conditions for its addition needed to be determined. Similarly, the rate with which power was increased in relation to the pressure had a substantial effect on the stability of the plasma, and as such, changing this rate enabled some control over the shape and position of the plasma. At low pressures, the plasma would often be positioned either on the anode or to one side of the substrate, as shown in figure 3.2.

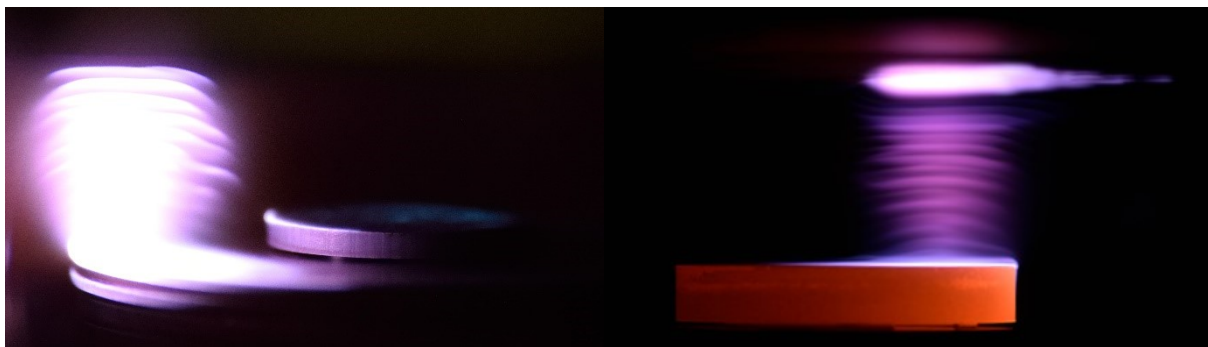


Figure 3.2: Photographs of pure H_2 plasmas at low pressures (40-80 Torr), with the plasma on the anode (left) and on one side of the substrate (right).

However, once the plasma was uniform, it would generally remain stable more easily, and the characteristic regions of a DC plasma discharge became identifiable, shown in figure 3.3.

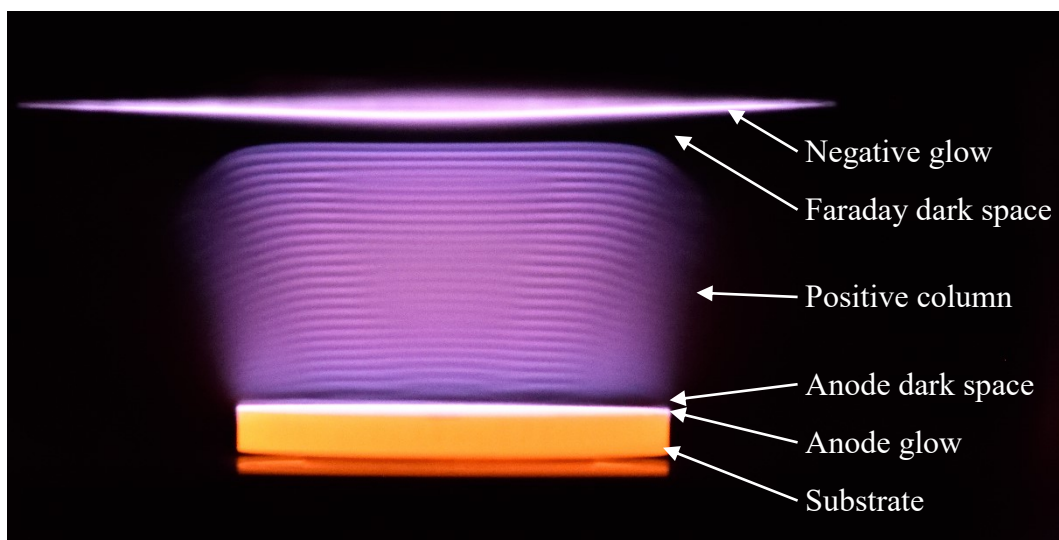


Figure 3.3: Photograph of a pure H_2 plasma at 100 Torr, annotated with features.

The negative glow is too bright to be able to see other features, such as the Aston dark space, the cathode glow and the cathode dark space, where secondary electrons are produced from ions impacting the cathode and accelerated by the potential field. The negative glow is the result of a high density of electrons colliding, emitting radiation. The Faraday dark space is an area in which there are sufficiently few gas species that electrons are able to travel through to the positive column without a collision, hence the lack of radiation [73]. Once in the positive column, the gas pressure is sufficient for collisions to occur, and as such, the positive column is where the gas species are activated for CVD. The anode glow results from electrons being attracted to and ions being repelled from the positively charged anode causing an increased potential field on the anode, and a decrease in electron density directly above it – the anode dark space. The “striations” – the layering pattern of bright and dark regions – in the positive column act similarly to a standing wave, with changing the frequency of the pulses altering the spacing between them, and result from electron bunching: a kinetic resonance effect occurring with the use of DC discharges in gases.

Addition of CH₄ resulted in a green glow in the middle of the purple H₂ plasma, indicating the presence of C₂ species, which have a distinct optical emission of 516 nm, shown in figure 3.4. Using optical emission spectroscopy, the intensity of this peak was seen to increase over time relative to the H_α and H_β peaks at 656 nm and 486 nm respectively (which cause the purple colour of the pure H₂ plasma). This is most likely due to the reactor slowly accumulating C₂ radicals within the plasma, as a result of the outward flow being biased towards lighter species causing a slow increase in the partial pressure of CH₄ in the chamber.



Figure 3.4: Photographs of CH₄/H₂ plasma (t is time after CH₄ addition):

Left: $t = 3$ min, 130 Torr, 2.5 kW

Centre: $t = 10$ min, 180 Torr, 3.5 kW

Right: $t = 25$ min, 180 Torr, 5.25 kW

Having gained some familiarity with obtaining stable H₂ plasmas while developing the cleaning method, maintaining stability on addition of CH₄ became the next series of experiments.

CH₄ was initially added when at deposition conditions, 170-200 Torr. However, this usually resulted in the plasma shrinking rapidly and forming an arc. Introduction of CH₄ at a lower flow rate than usual (*e.g.* 5 sccm rather than 20 sccm) resulted in a similar effect, albeit over a slightly longer duration of a few minutes. Subsequently, addition was performed at a range of pressures, from 50-150 Torr. At lower pressures, it was observed that the addition of CH₄ actually helped to stabilise the plasma rather than making unstable, causing the plasma to broaden into a total uniform coverage of the substrate, and maintained this stability when the pressure was then increased. 100 Torr (at 2 kW) was determined to be optimal pressure.

However, this required the plasma to be on the substrate at the point of CH₄ addition and not on the anode. The prior work on ensuring a cleaner, and hence more conductive, cathode helped with this, as the plasma was unlikely to form over the substrate when a less resistive path could be found between the uncoated outer areas of the cathode and the anode: when the plasma did form on the substrate, the shape was not of an even cylindrical field, but more like that of an inverted bell, with no negative glow in the centre of the cathode, forming a ring further out instead.

In order to ensure the plasma quickly formed on the substrate, regular cleaning runs were performed, but to aid in this, the power curve – the rate with which the power was increased relative to the pressure – was also increased. It was found that a much higher curve, especially at lower pressures, enabled more rapid formation of the plasma on the substrate, with values shown in table 3.1.

Table 3.1: Input power relative to pressure during PDR start-up.

Pressure / Torr	Power / kW	
	Previous	New
1.8	0.05	0.05
5	0.1	0.3
10	0.2	0.5
20	0.4	0.8
40	1	1

3.1.3 Cooling of the substrate and electrodes during deposition

With the improved start-up procedure enabling easier control over plasma position and the addition of CH₄ at 100 Torr assisting in forming uniform and stable plasmas, the next issue that was approached was the limited control over substrate temperature.

When replicating the deposition performed by predecessors, the substrate would glow “white-hot”, suggesting it was a much higher temperature than desired. This was supported by the appearance of the diamond films which were generated, shown in Chapter 3.2, with the morphology of diamond grown at too high a temperature [58]. As such, control over the temperature was crucial to achieving the high quality diamond growth required for radiation detection applications.

In the initial design, there were thermocouples attached to the anode and cathode, but over the course of the past 2 years, these were both damaged and rendered inoperable. A two-colour pyrometer was also used, but gave clearly erroneous temperature estimates, likely due to the radiation emitted from the plasma. With no means to assess the temperature quantitatively, a more qualitative method was employed, based partly on the “brightness” of the substrate’s glow and partly on the appearance of the diamond produced.

Adjustments to the temperature could be made in three main ways: by altering the distribution of water flow between the bell jar and the electrodes, by changing the size of the wire ring spacers, and by using a lower power.

Use of a lower power would result in less heating, but is not a viable method to reduce substrate temperature as lower powers would be unable to achieve the required potential field for deposition to occur; reducing the space between the electrodes would allow for the same potential field to be generated with a lower power, but has been shown to result in increased arcing [58], which is undesirable for DC CVD deposition.

As such, the first major step in reducing the substrate temperature was to direct more of the water cooling flow into the electrodes, reducing their temperature, from the bell jar. When constructed, the water cooling apparatus was fitted with a tap to control the water flow into the bell jar, which, when closed, increased the flow into the cathode and anode’s water-cooled plates. Doing so achieved a visible reduction in the substrate temperature, with it glowing less brightly for a given power and pressure; this also reduced the outlet water temperature by *ca.* 10 °C, allowing for the power to be further increased when required without the danger of

bursting the PFA pipes in the water cooling system. Alongside this, deposition was only performed when the adjacent MWCVD reactor, which uses the same water chiller, was disconnected from the water cooling system, which reduced outlet temperatures by a further 3 °C, providing even more capacity to increase the operational power.

Further to these changes, with the substrate temperature judged to still be too high, and on the suggestion of Dr. Fox, the wire rings spacers were changed. The Ta spacer (0.5 mm diameter) between the substrate and the Mo anode was replaced with a thinner one (0.25 mm diameter) and the spacer between the anode and the Cu plate was removed entirely. By reducing the wire thickness, the thermal conduction between the substrate and the anode was improved significantly, with the conduction between the anode and Cu plate improved even further by having no wire. The subsequent growth run was visibly cooler, with the substrate glowing orange as shown in figure 3.5, suggesting a temperature closer to the optimal growth temperature of 900-1000 °C. A further run was then carried out using a 0.25 mm diameter W wire between the substrate and anode, producing similar results. The diamond grown during these runs is characterised and discussed in Chapter 3.2.



Figure 3.5: Photograph of a CH₄/H₂ plasma at 200 Torr, 3.3 kW, 12 minutes after the addition of CH₄. The ring spacer was 0.5 mm diameter, and as such, the space between the anode and the substrate is harder to see.

3.2 Diamond growth and characterisation

Herein, the diamond samples will be denoted as sample 1, sample 2 *etc.* as outlined in table 3.2 below. Raman spectra are only available for a few samples due to limited equipment availability and the limited number of substrates for use.

Samples 1 and 2 were performed before the establishment of the cleaning procedure outlined in Chapter 3.1.1, and they were also before the changes improving plasma stability were known: all had stable plasma, but there were many runs which were attempted which resulted in loss of plasma stability of duration less than 3 minutes, which are not recorded here.

Table 3.2: Diamond samples grown in the PDR during the experimental work mentioned in Chapter 3.1. Depositions ending with arcing or the water cooling exceeding safe temperatures denoted by an asterisk (*) and a dagger (†) respectively in the “Deposition duration” column.

Sample number	Pressure / Torr	Initial power / kW	Initial voltage / V	Final power / kW	Final voltage / V	Deposition duration / min
1	175	3.25	613	3.85	590	55*
2	200	3.09	627	3.03	615	33
3	175	3.50	601	4.00	_h	29*
4	175	3.30	605	5.50	563	63
5	175	4.25	588	5.25	582	27
6	175	3.30	596	6.00	601	55
7	175-200	3.25	616	4.50	591	30*
8	200	3.30	626	4.75	593	29*
9	200	3.25	606	4.00	580	24
10	200	3.25	604	4.25	572	16

^h Arcing occurred and the power supply was switched off before the voltage was read.

Sample 1:

Sample 1 was produced using a step-wise increase in pressure, with CH₄ added at 175 Torr. The plasma was very stable and uniform across the surface. The green glow was initially observed at 125 Torr, with an increasing presence as pressure rose. When 175 Torr was attained, the voltage was 613 V with a power of 3.25 kW, and the power was increased to maintain the voltage above 610 V. After 55 minutes, the plasma arced, with the voltage having dropped below 600 V and the water cooling reaching temperatures prohibiting further power increases.

The SEM images (figure 3.6) show that diamond was nucleated, but with inconsistent surface orientations. This sample was saved until the Raman spectrometer was available, so Raman spectra are available, shown in figures 3.7 and 3.8. As shown in the spectra, the diamond is to a varying quality, with the nucleation analysed in figure 3.8 not featuring a significant graphite peak, while figure 3.7 shows a high graphite impurity.

Given the quality of diamond grown, the method used in this was kept as a consideration for all future growth.

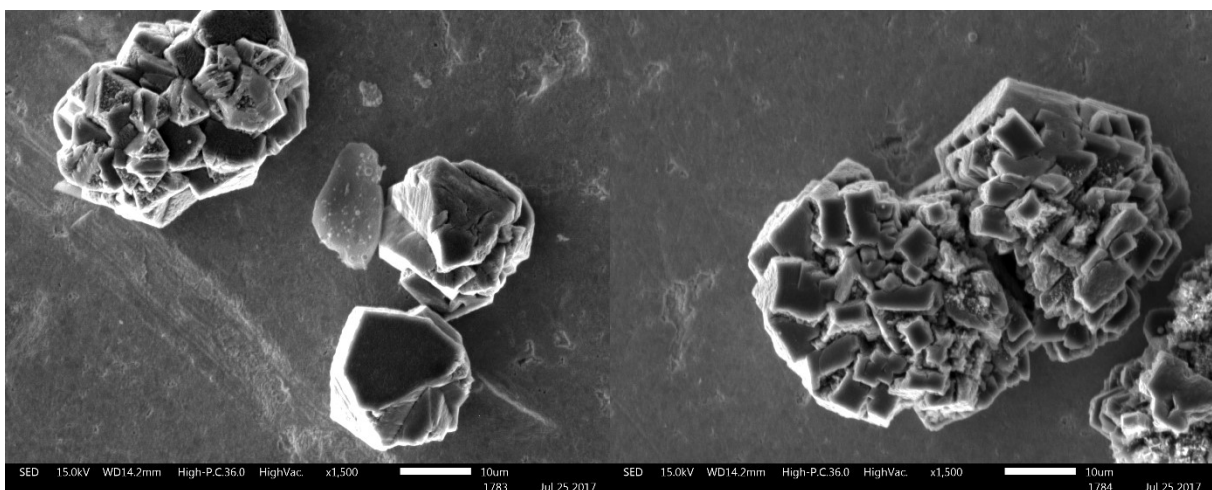


Figure 3.6: SEM images of sample 1 showing two different areas of diamond nucleation.

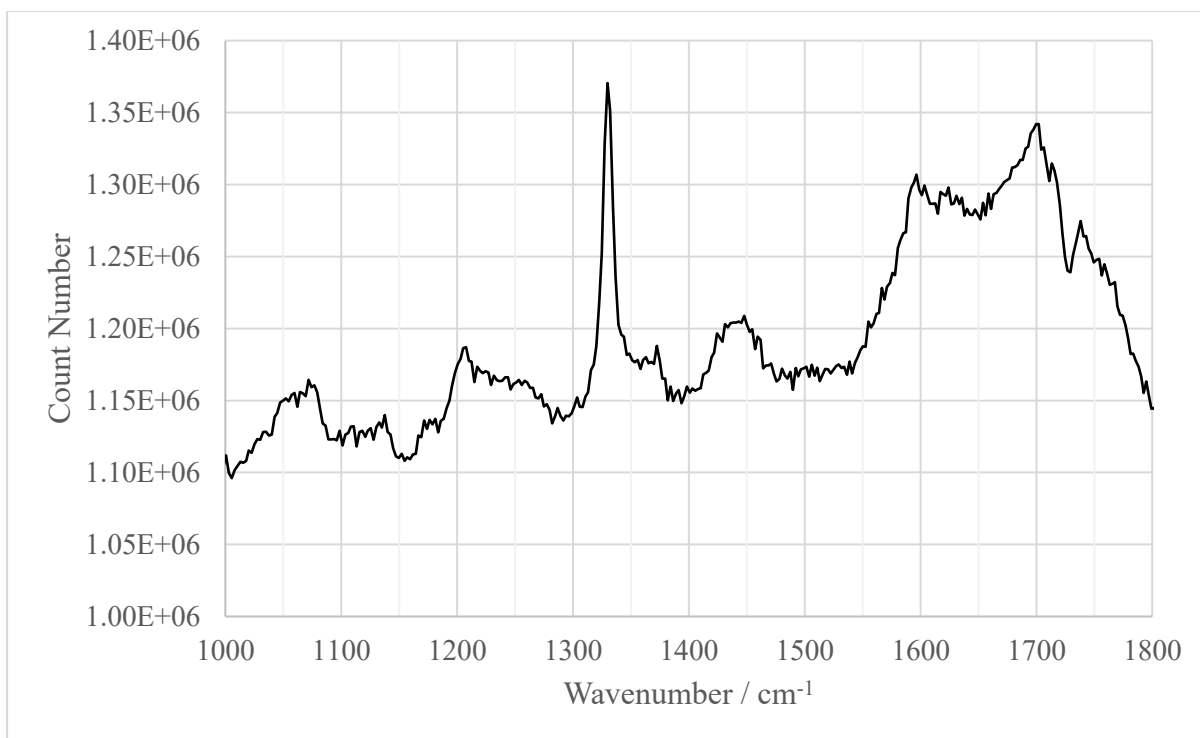


Figure 3.7: Raman spectrum of a diamond nucleation on sample 1. Diamond peak at 1329.8 cm^{-1} , FWHM 11.3 cm^{-1} ; graphite peak at 1594.3 cm^{-1} .

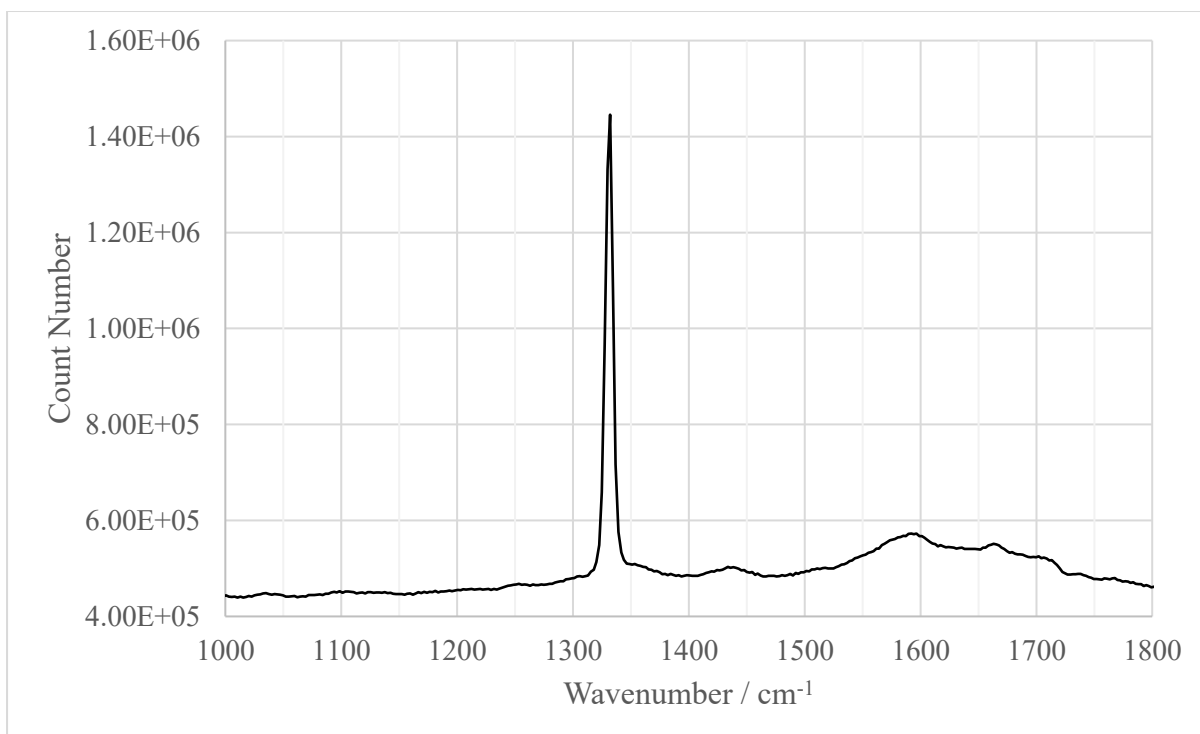


Figure 3.8: Raman spectrum of a diamond nucleation on sample 1. Diamond peak at 1332.2 cm^{-1} , FWHM 7.3 cm^{-1} .

Sample 2:

Sample 2 was grown using the “current control” mode, in an attempt to maintain a more stable potential field across the electrodes. An attempt was made using the “voltage control” mode, but a plasma could not be struck, as the power supply does not provide the “ignition capacity” when using this mode.

The pressure was increased step-wise with CH₄ added at 200 Torr. Given the lack of control over the power, the current was increased cautiously, but resulted in a stable and uniform plasma. When the pressure stabilised at 200 Torr, the current was set to 4.92 A, resulting in a power of 3.09 kW and voltage of 627 V, which remained fairly constant. These conditions seemed ideal, but as the plasma began to shrink after 30 minutes, the power was switched off due to fears of arcing and not being certain what would happen if an arc occurred in “current control” mode, which had not been used before. After consulting with Dr. Smith, it was decided to not use “current control” mode again, for fear of damage to the power supply in the event of an arc.

However, upon inspection of SEM images, shown in figure 3.9, it was apparent that no diamond had nucleated.



Figure 3.9: SEM image of the surface of sample 2. The material on the surface is dirt, rather than diamond nucleation, shown to give perspective of the surface.

Sample 3:

Sample 3 was an attempt to recreate the growth conditions used for sample 1. A cleaning run, using the stacked tower of substrates method outlined in Chapter 3.1.1, was performed immediately before growth.

Sample 3 is also the first sample which had CH₄ added at 100 Torr, which may have led to increased graphite impurities, but these should have been etched by the atomic hydrogen in the plasma before diamond deposition began. The process proceeded as expected, with similar plasma stability and positioning as sample 1 had, but with a lower voltage than before. After 29 minutes, the plasma arced, and the power supply was switched off, before the voltage was read: as such, the “end” voltage is not known.

Figure 3.10, showing an SEM image from sample 3, shows successful nucleation of nanodiamond and formation of a thin diamond film. However, the morphology suggests that the growth temperature was too high, hence the lack of definition of the surface orientations.

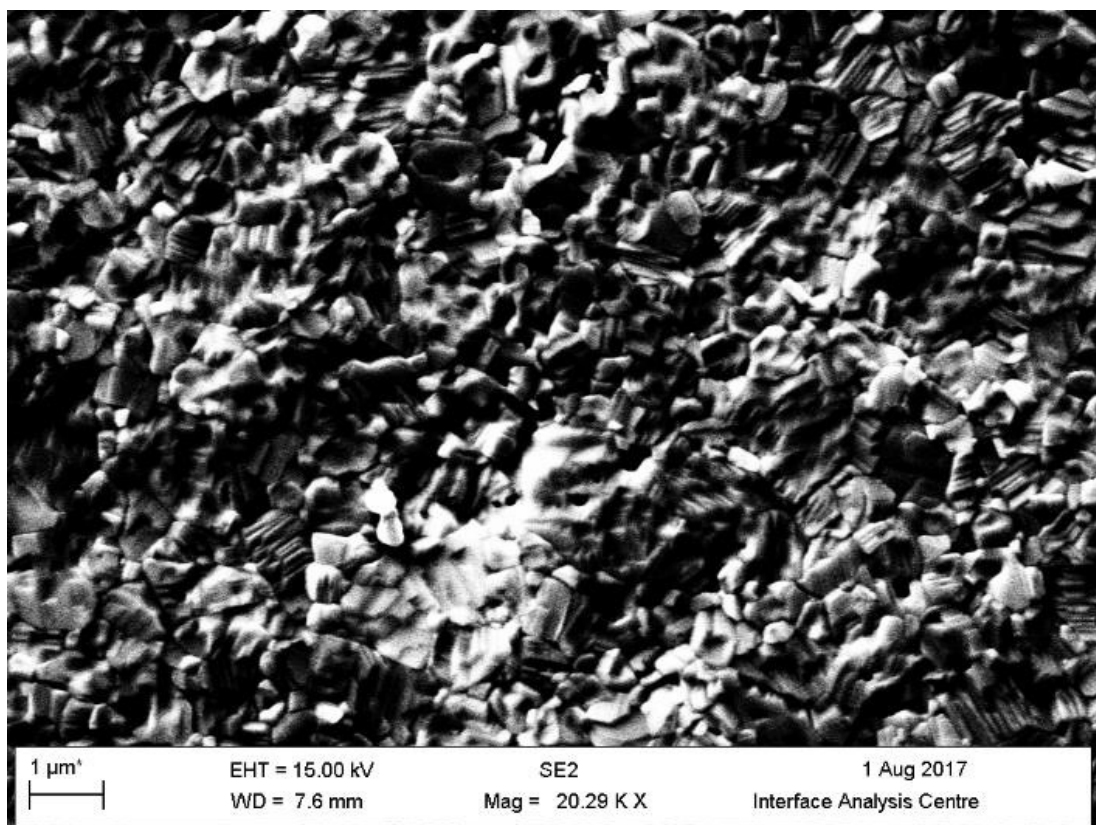


Figure 3.10: SEM image of the surface of sample 3, showing a thin film of nanocrystalline diamond forming, with a lack of surface orientation due to the high growth temperature.

Samples 4 and 5:

Sample 5 marked the beginning of experiments into manipulation of the substrate temperatures by modifying the water cooling flow to the electrodes. During the growth of sample 4, the water flow was increasing restricted to the bell jar, resulting in lower temperatures being seen for the electrode water outlets. With an improved balance of water flow distribution between the electrodes and the bell jar, sample 5 was run. Sample 5 failed to reach a sufficient potential field initially, so the power was increased substantially, utilising the new capacity for higher powers without damaging the water cooling system.

Figures 3.11 and 3.12, showing SEM images for samples 4 and 5 respectively, both show similar high temperature growth morphologies, suggesting that further work needed to be done to reduce the substrate temperatures. However, sample 5 has more defined grain boundaries, implying a better growth temperature than sample 4.

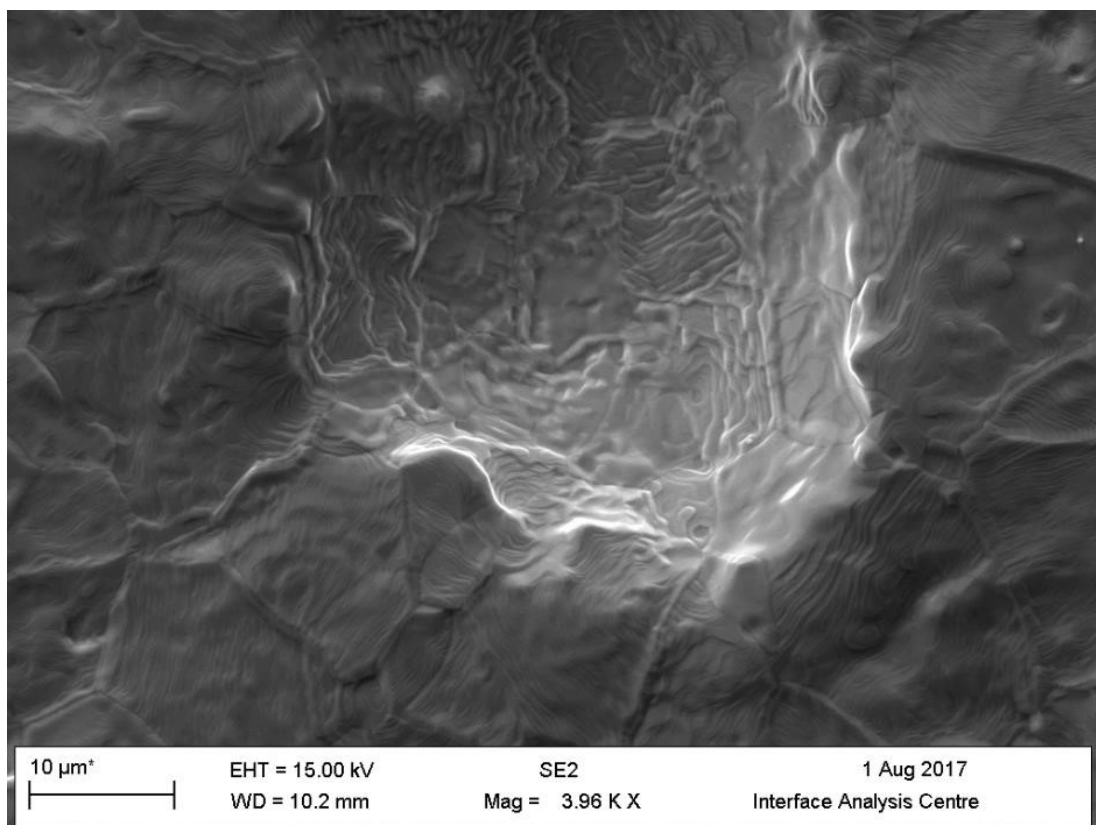


Figure 3.11: SEM image of the surface of sample 4, showing a thin film with a lack of surface orientation due to the high growth temperature.

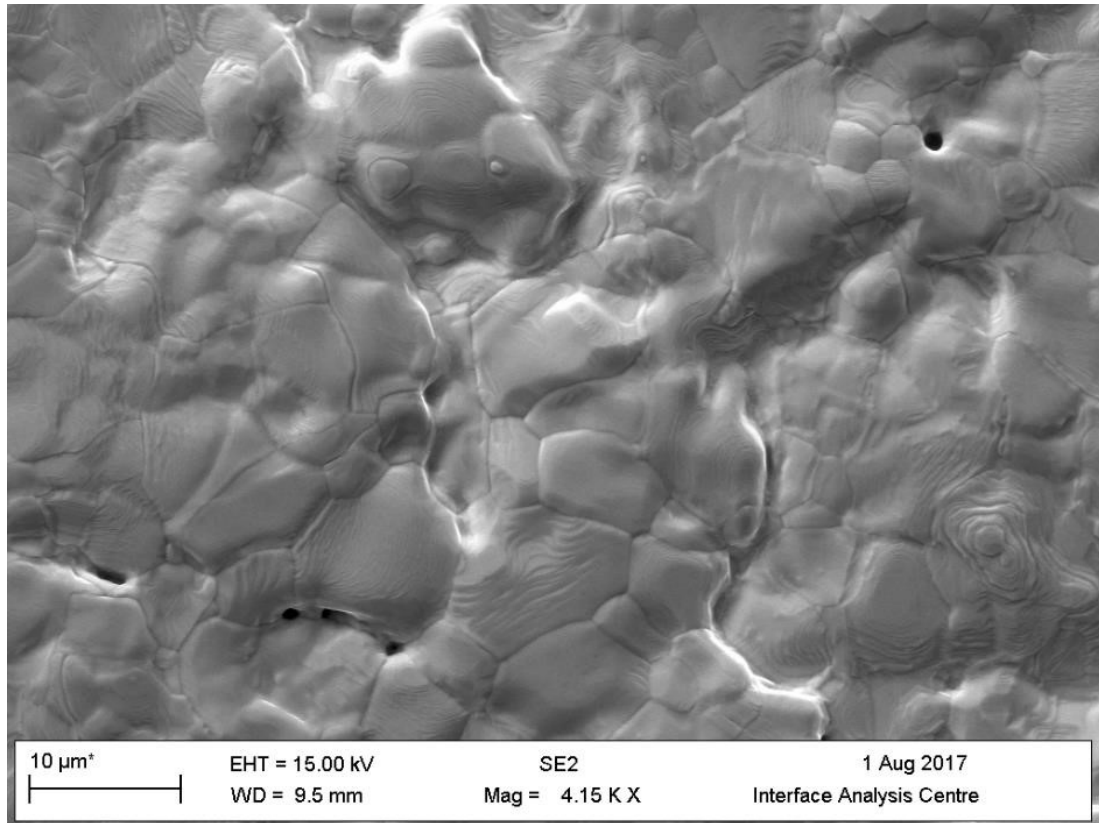


Figure 3.12: SEM image of the surface of sample 5, with more defined grain boundaries than seen in sample 4, suggesting a lower growth temperature, although still higher than required for high quality diamond growth.

Sample 6:

In an effort to achieve reproducibility, sample 6 was run at the same conditions as sample 4, but, as was common with the PDR, produced very different deposition conditions than those of sample 4's run. With the improved cooling water flow, the power could be increased higher than before, but this effective led to an increased current with little increase in voltage. However, as shown in figure 3.13, the surface of sample 6 was similar to the surface of sample 4, with ill-defined crystal grains, but a film grown nonetheless.

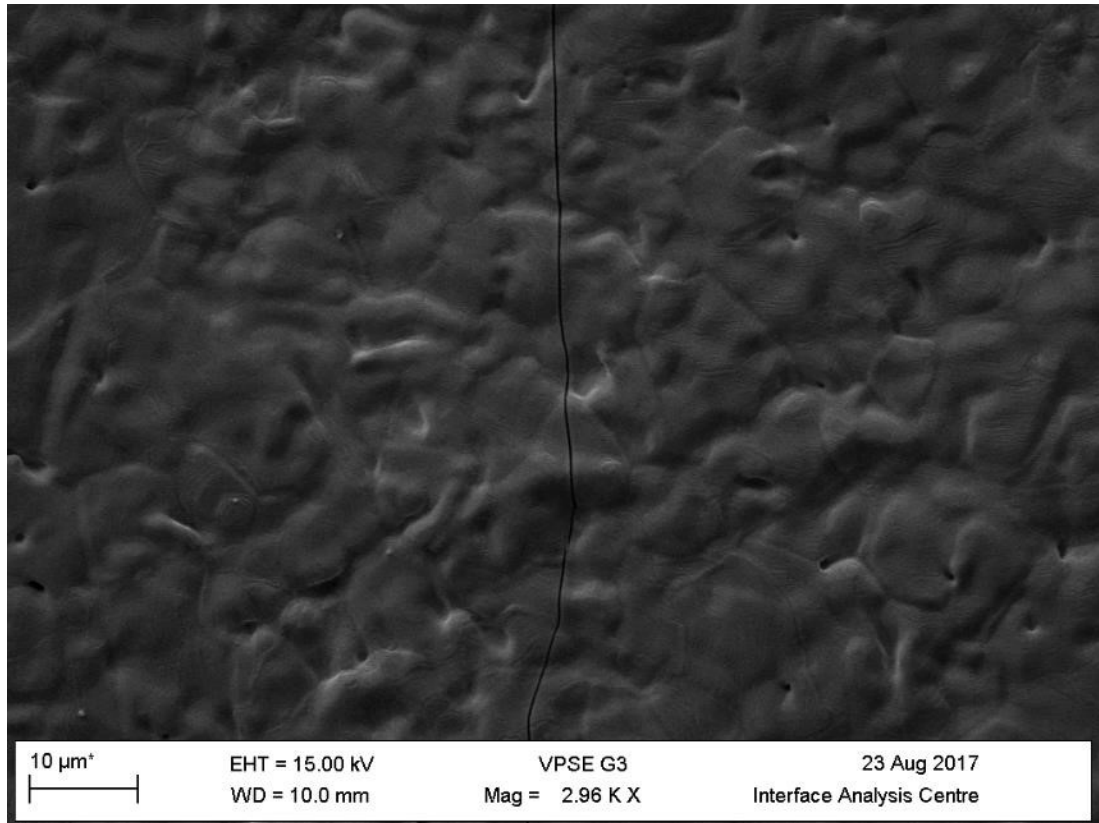


Figure 3.13: SEM image of the surface of sample 6, with a similar surface to that of sample 4.

Sample 7:

Sample 7 was carried out the same as sample 6, but, again, due to the inconsistent nature of the PDR, a much higher voltage was achieved. In order to utilize this, another idea was tested: to compensate for a decreasing voltage, the pressure would be increased, rather than the power. After 22 minutes, the voltage was dropping below 610 V, so the pressure was increased to 200 Torr. Initially, this was successful, raising the voltage without increasing the power. However, during the pressure cycle, in which the automated pressure control would overshoot the “set pressure” by *ca.* 10 Torr and then decrease again to the input value, the voltage dropped rapidly as soon as the pressure began to drop for 210 Torr to 200 Torr. This drop in voltage shrank the plasma, so it was no longer stable or uniform, so the power was turned off to avoid arcing.

Some small nucleation was observed on the surface, as shown in figure 3.16, and Raman spectra were obtained for some of these diamond crystals, in figures 3.14 and 3.15.

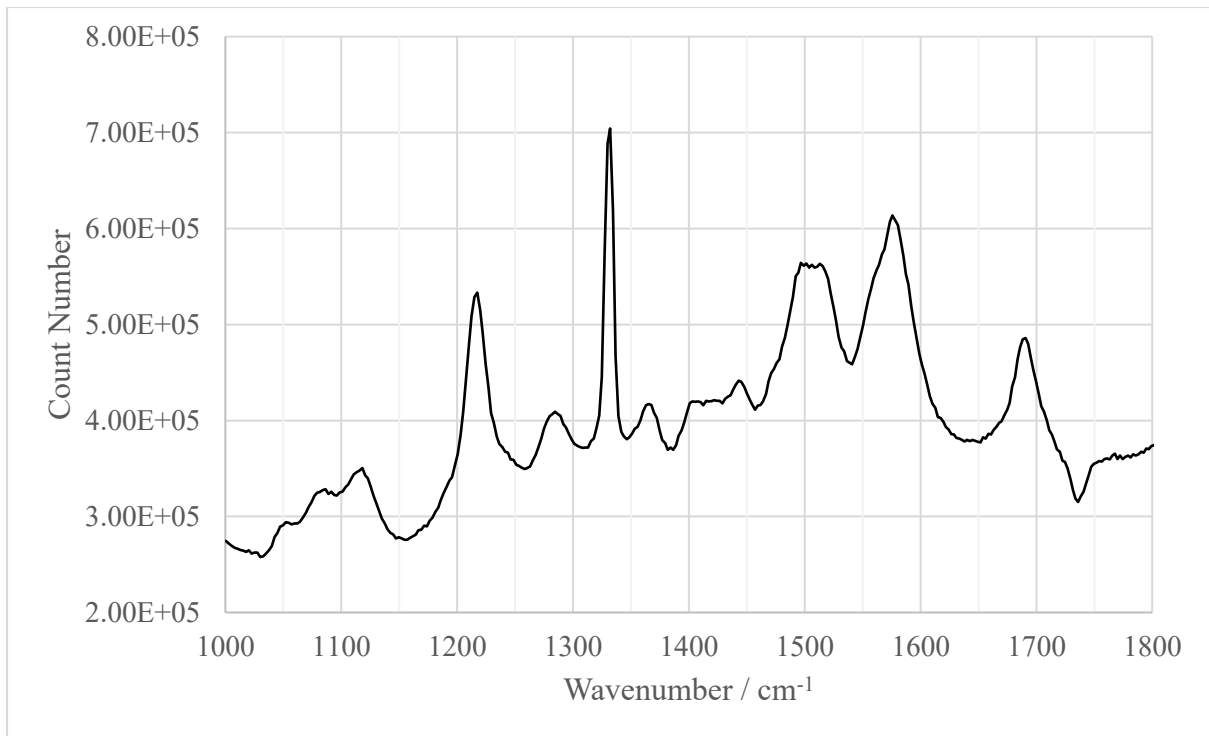


Figure 3.14: Raman spectrum of a diamond nucleation on sample 7. Diamond peak at 1331.3 cm^{-1} , FWHM 8.8 cm^{-1} ; graphite peak at 1578.1 cm^{-1} .

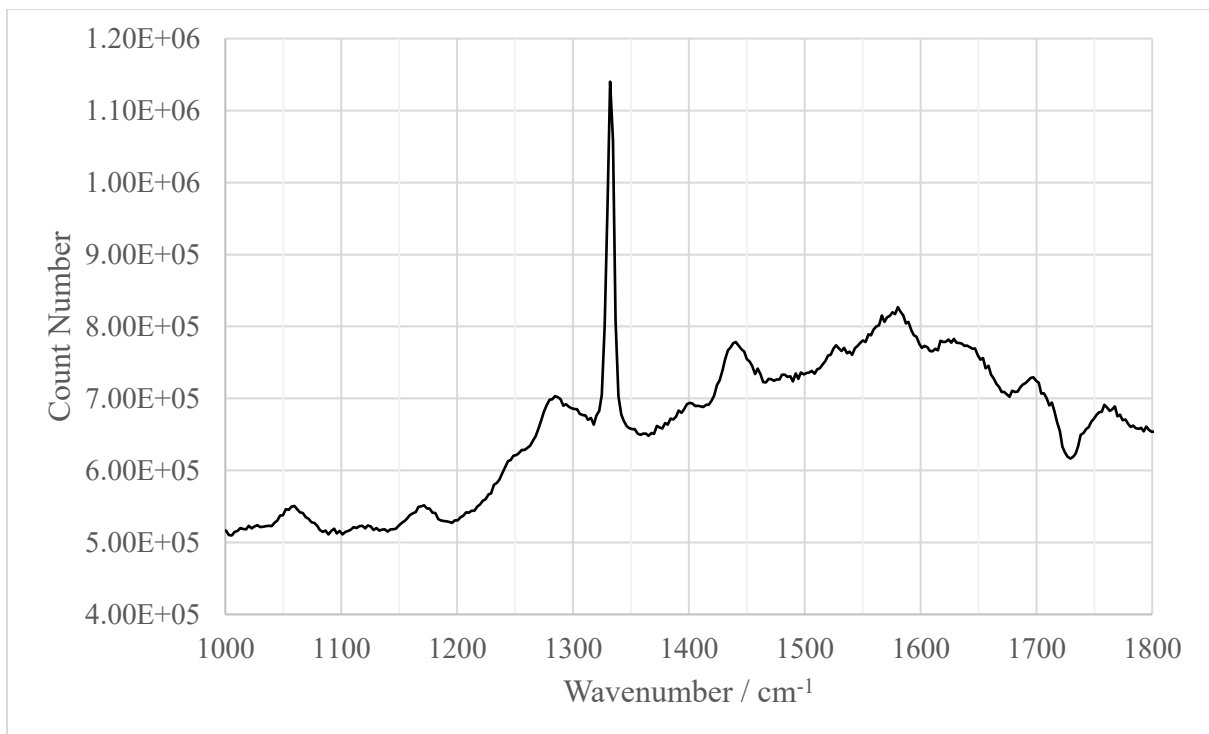


Figure 3.15: Raman spectrum of a diamond nucleation on sample 7. Diamond peak at 1332.2 cm^{-1} , FWHM 11.3 cm^{-1} ; graphite peak at 1585.1 cm^{-1} .

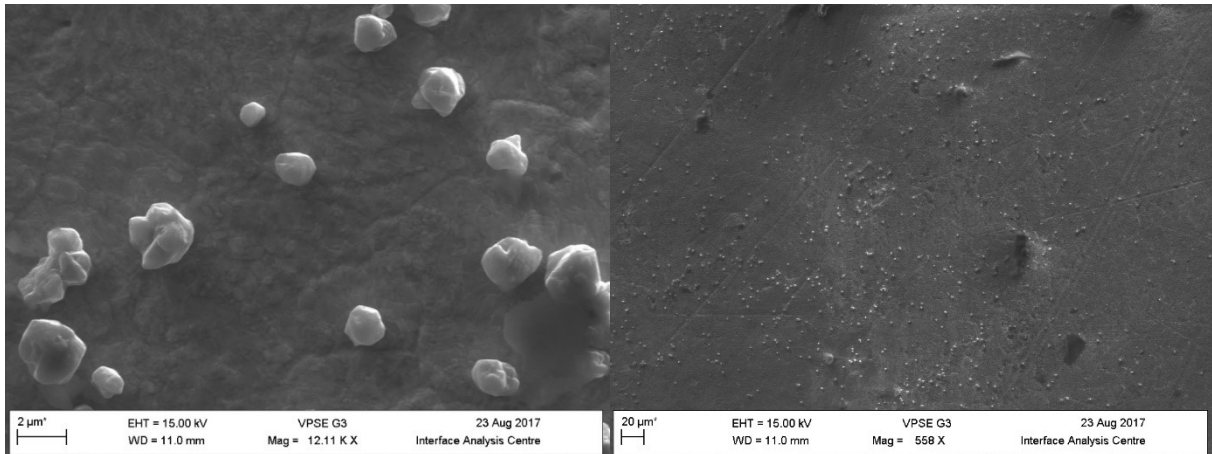


Figure 3.16: SEM images of the surface of sample 7, showing very small diamond nucleation.

As shown by the Raman spectra, the nucleations are good quality diamond, with low FWHM values for each, but both contain a significant graphite impurity peak. This sample shows that the PDR certainly has the capacity for good diamond growth, and only lack the consistency to generate this on a more frequent basis.

Sample 8:

Sample 8 was an attempt to replicate the growth on sample 7, but, to avoid the pressure cycle's effect, the pressure would be initially set to go to 200 Torr. However, when these conditions were reached, the voltage began to drop rapidly, and after 29 minutes, the deposition had to be stopped before arcing occurred. SEM images showed a total absence of diamond growth.

Sample 9:

For sample 9, the adjustments to the use of wire ring spacers discussed in Chapter 3.1.3 were used. A pressure of 200 Torr was chosen, again, with the objective of replicating sample 7. With the improved cooling, it was apparent just from visual inspection that the temperature of the substrate was significantly lower. However, the power supply decreased the potential rapidly again, resulting in a shorter growth run than desired.

SEM images, figures 3.17 and 3.18, showed extensive nucleation of microcrystalline diamond, with distinct triangular (111) surfaces. (111) orientation surfaces suggest a lower temperature

than desired, but given the quality and quantity of diamond crystals, the reduced insulation has certainly improved growth, as confirmed by Raman spectroscopy – figures 3.19 and 3.20.

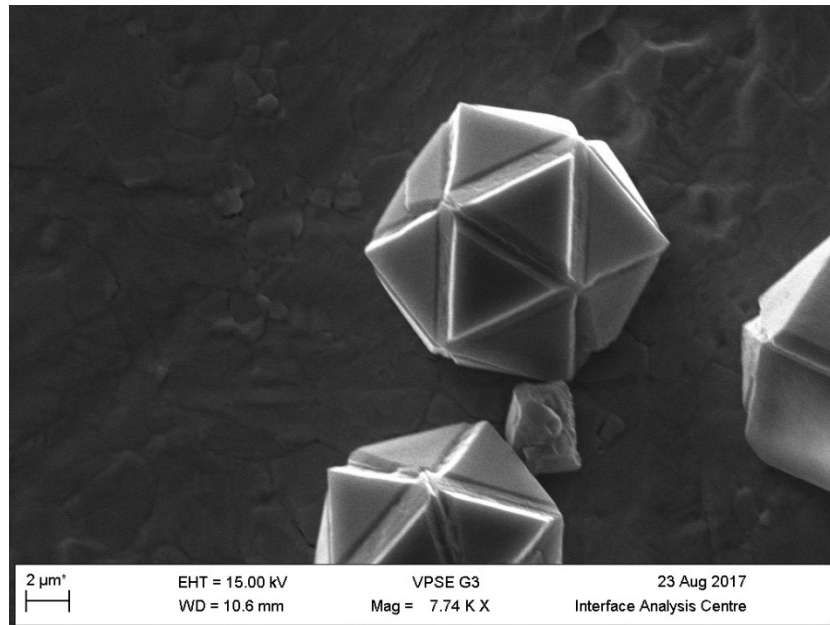


Figure 3.17: SEM image of a diamond crystal on the surface of sample 9, with distinct triangular (111) orientation.

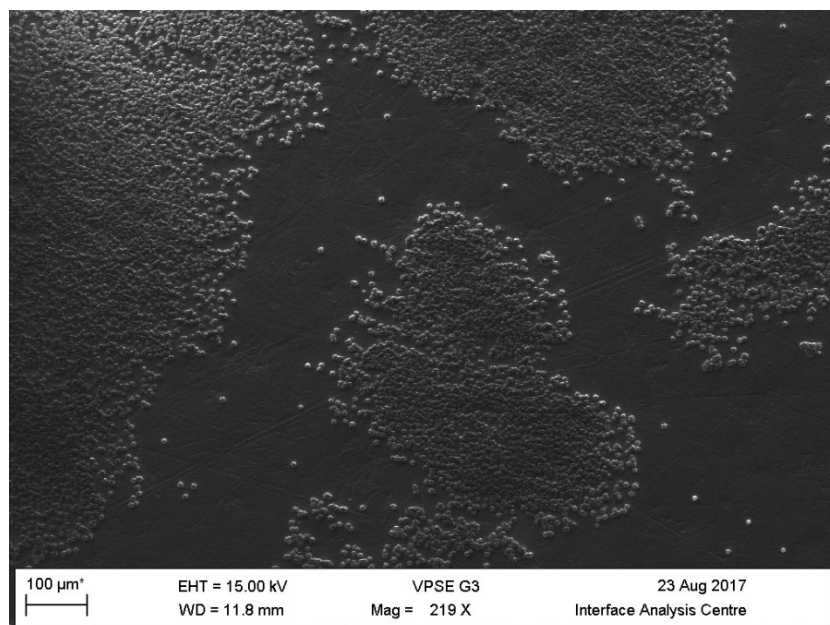


Figure 3.18: SEM image of the surface of sample 9, showing the thick dispersal of diamond crystals.

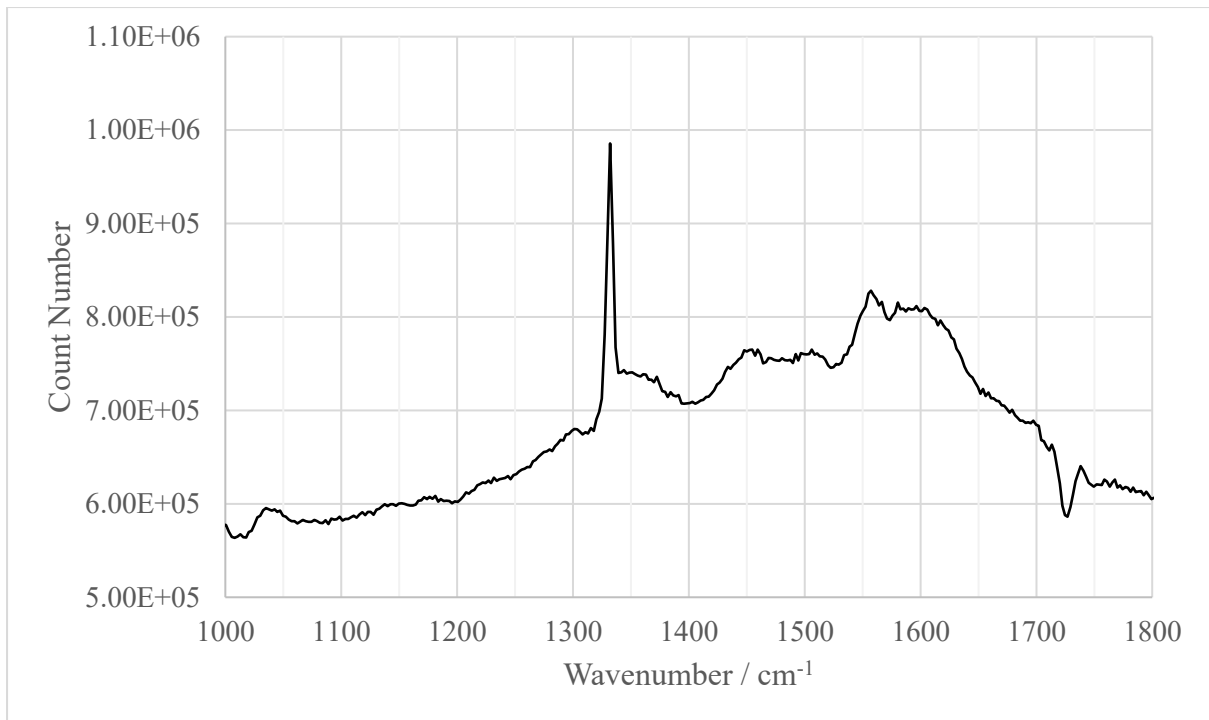


Figure 3.19: Raman spectrum of a diamond crystal on sample 9. Diamond peak at 1332.1 cm^{-1} , FWHM 6.5 cm^{-1} ; graphite peak at 1580.6 cm^{-1} .

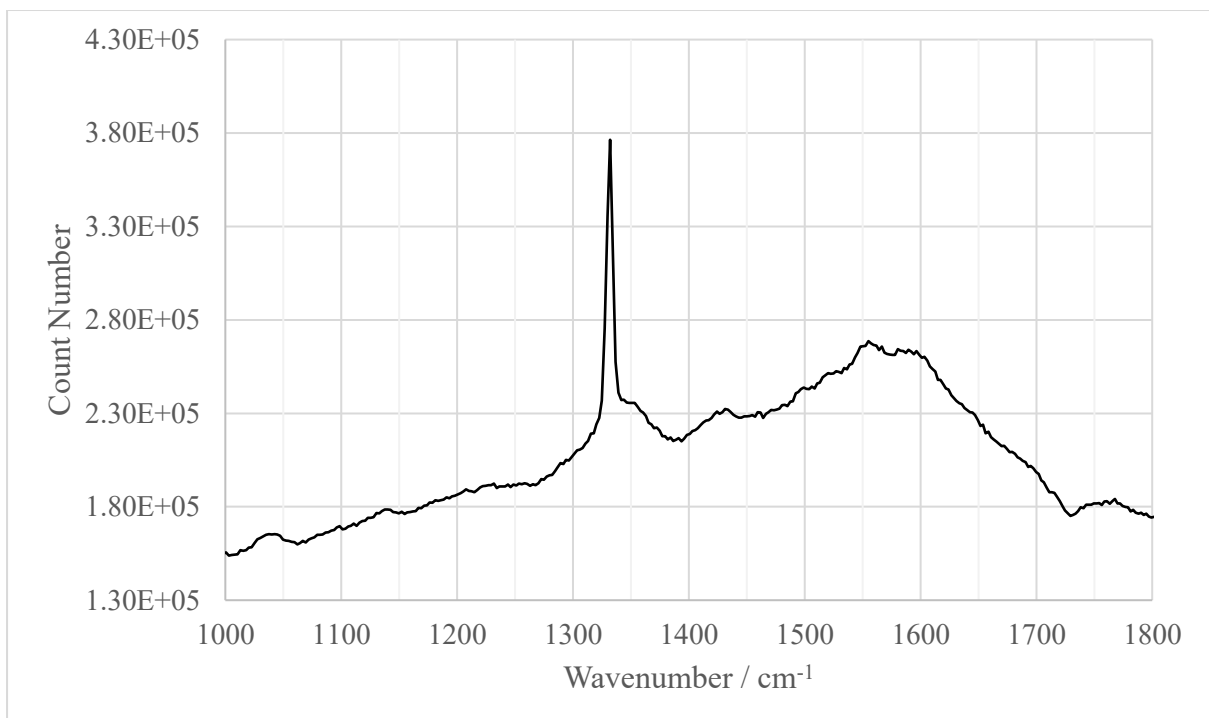


Figure 3.20: Raman spectrum of a diamond crystal on sample 9. Diamond peak at 1331.2 cm^{-1} , FWHM 7.2 cm^{-1} ; broad graphite peak at 1553.0 cm^{-1} .

These Raman spectra support the quality of the diamond grown, as the diamond peak is narrow in both, and the purity as the graphite peak is considerably lower in intensity – especially when considering that the sp^2 graphite has a higher response to the 514 nm Raman laser used than the sp^3 diamond.

Sample 10:

With the improved diamond quality produced by sample 9, sample 10 aimed at replicating the deposition. However, the growth period was shorter due to the voltage dropping at a faster rate than was seen for sample 9.

Both SEM images – figures 3.21 and 3.22 – and Raman spectra – figures 3.23 and 3.24 – support the assertion that diamond of a slightly lower quality but similar size were grown on sample 10, showing, for the first time, consistent, consecutive good quality deposition can be performed: an important first step towards the production of consistent high quality diamond films.

No further deposition runs were performed due to time constraints, but with some consistency achieved, future work on the PDR should begin to yield better quality diamond than has been produced before more easily.

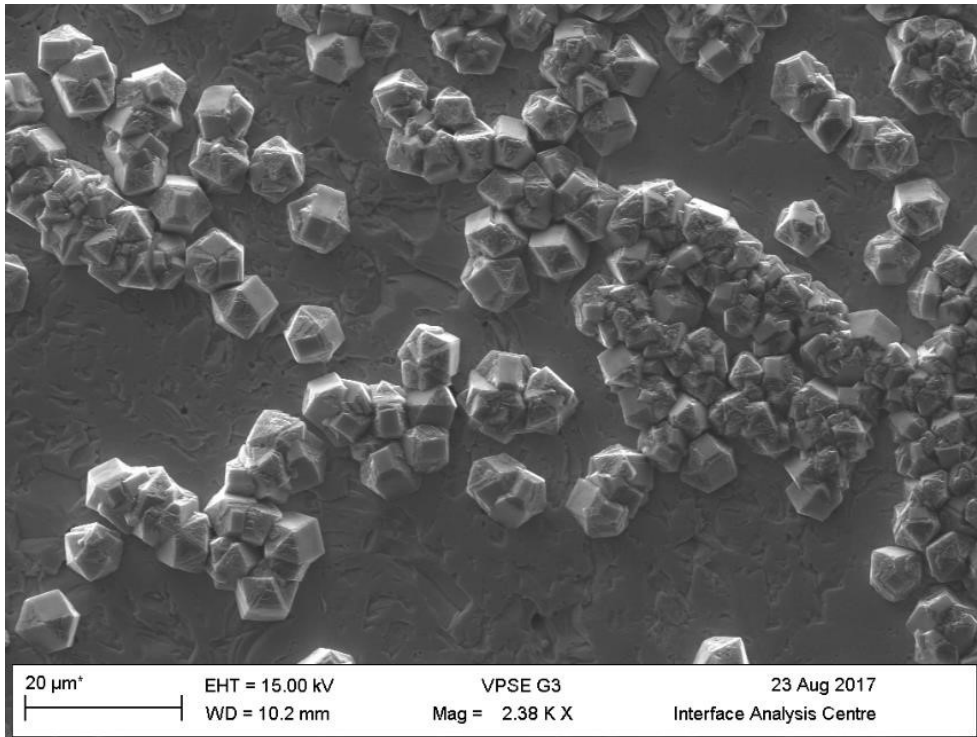


Figure 3.21: SEM image of the diamond nucleation on the surface of sample 10, which shows diamond of a similar size and shape to that produced by sample 9.

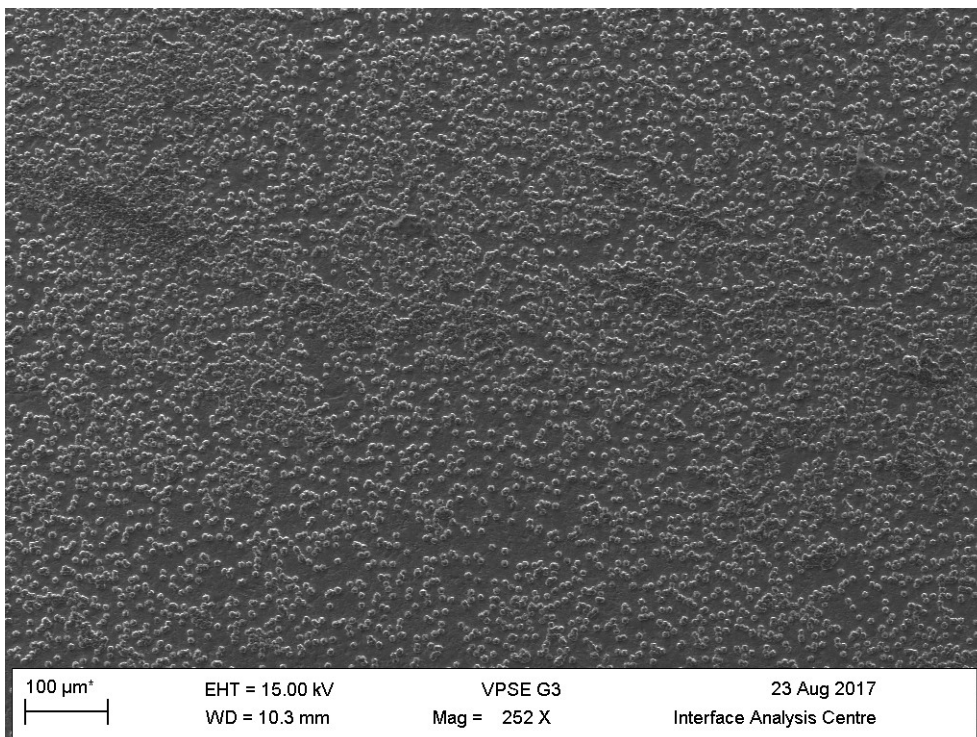


Figure 3.22: SEM image of the surface of sample 10, which shows similar distribution to the diamond grown on sample 9.

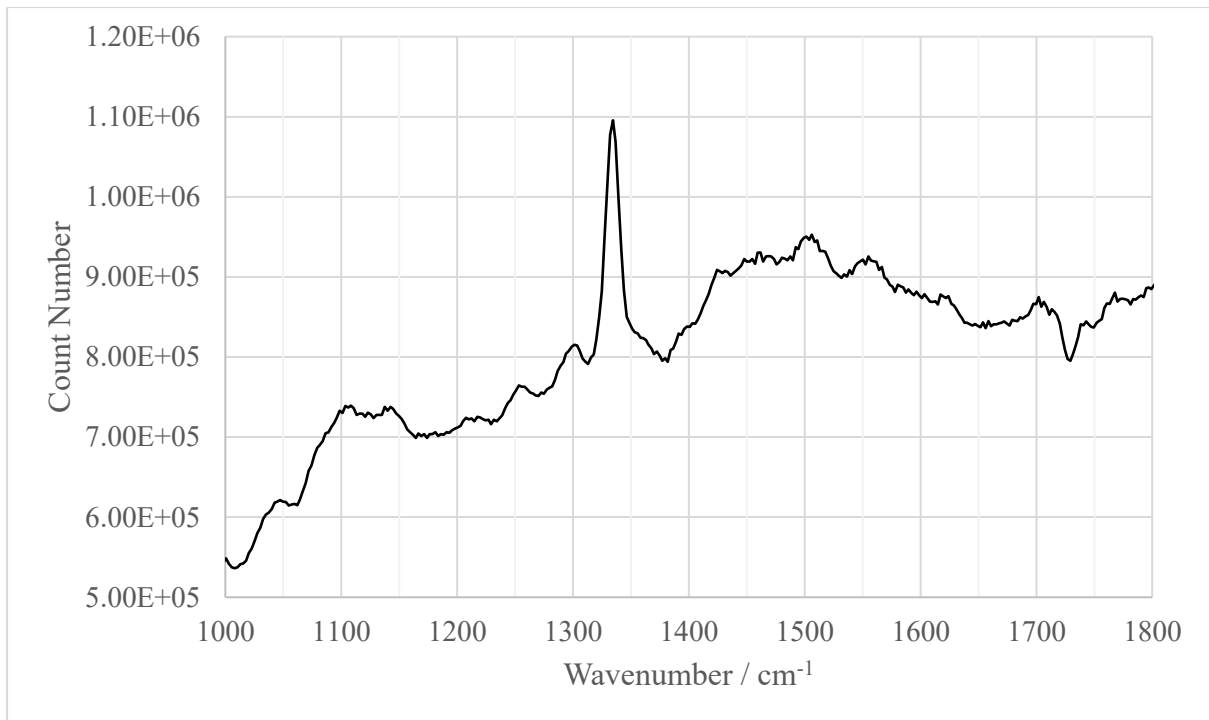


Figure 3.23: Raman spectrum of a diamond crystal on sample 10. Diamond peak at 1334.3 cm^{-1} , FWHM 13.9 cm^{-1} ; broad graphite peak at 1583.0 cm^{-1} .

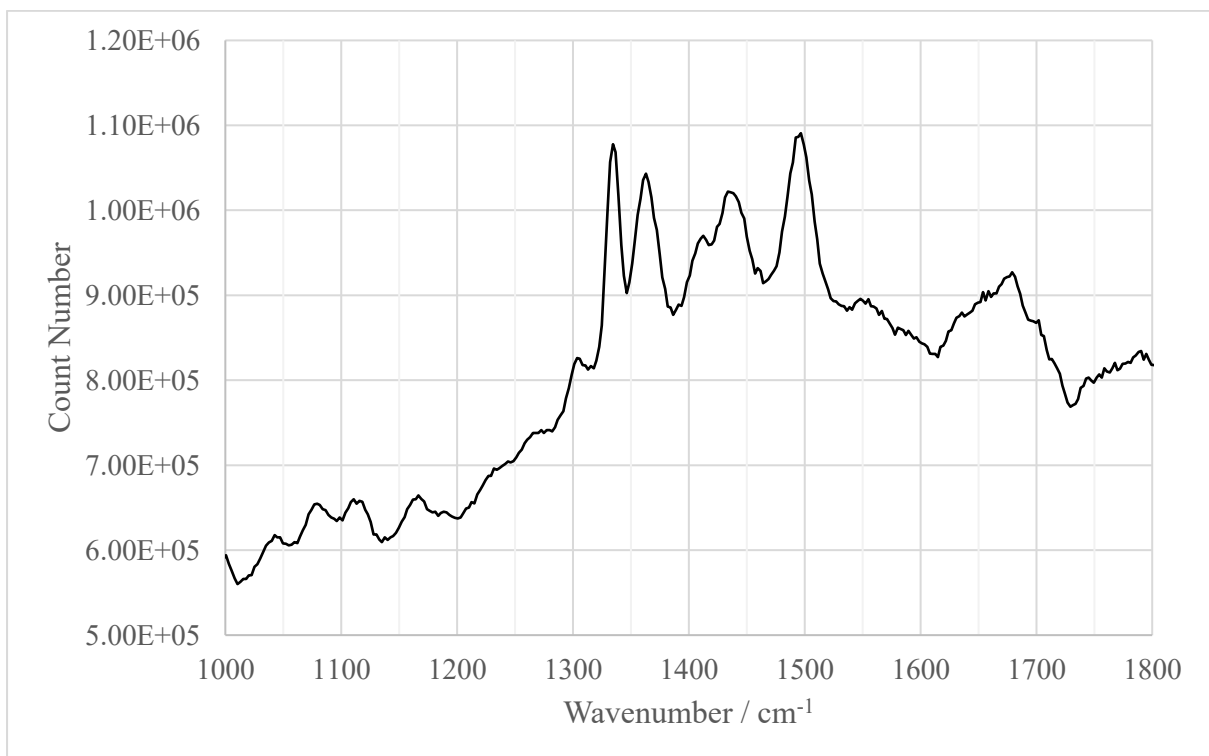


Figure 3.24: Raman spectrum of a diamond crystal on sample 10. Diamond peak at 1334.3 cm^{-1} , FWHM 12.2 cm^{-1} ; no significant graphite peak, but a “disordered graphite” peak at 1364.1 cm^{-1} .

Chapter 4: Conclusions and Future Research

4.1 Summary

The primary aim of the research was to further optimize the PDR. Building on the work of predecessors, initial growth conditions were chosen and areas for optimization were selected based on experimental observations of the issues with achieving a reproducible system.

Initially, a new cleaning method was devised to remove residual deposits from both the cathode and substrates, enabling more consistent initial conditions of those components. The method has now become standard operating procedure and is carried out on a regular basis.

Subsequently, plasma stability was investigated. Having managed to make stable plasmas of pure H₂, CH₄ was added at various pressures to find the optimal conditions for CH₄ addition, determined to be 100 Torr and 2 kW. To further improve the repeatability of the deposition apparatus, a quicker increase in power relative to pressure was utilized. Combined with the cleaning method, this resulted in consistent, stable, central and uniform plasmas on the substrate.

The temperature of the substrate was focussed on, reducing the temperature significantly by changing the wire ring spacers used, resulting in a temperature closer to the temperature desired for high quality diamond growth. Alongside this, adjustments to the cooling of the electrodes allowed for higher powers to be used when necessary, facilitating more flexibility of the PDR to achieve optimal growth conditions.

Mixed results were produced by the deposition runs, mostly due to run-to-run inconsistencies of the PDR, but the final two runs produced similar distribution of similar high quality diamond crystals, suggesting that the conditions used are approaching the optimal growth conditions. The quality of the diamond is supported by Raman spectroscopy, with a peak at 1332.1 cm⁻¹ with FWHM of 6.5 cm⁻¹, which is consistent with the values produced by literature sources. These growth runs have been hindered by the rapid rate with which the potential field decreases: some further investigation into the operation of the power supply may resolve this.

Overall, the PDR has been optimized further, but is still not able to produce reproducible growth. With further work focussed on the areas outlined in Chapter 4.2, the PDR should be producing the desired high quality diamond films: once that has been achieved, isotopically pure ¹³C diamond can be easily produced for radiation detection devices.

4.2 Future work

Future work should be pursued on three fronts:

Further optimization of the experimental process, with particular focus to the change in potential field over time, may permit longer deposition runs. Similarly, the pulse duration could be varied, as suggested in other research [40], to alter the kinetics of the plasma, and thus its stability and chemistry, possibly resulting in better deposition conditions.

New electrodes have been designed and, at the time of writing, are being constructed. These new tungsten electrodes should help in stabilising the plasma and allow for better control of substrate temperature.

Finally, gas cooling should be investigated. The current water cooling system is difficult to control, so the development of a gas cooling system with a variable pumping rate would allow for much more precise control over the substrate and electrode temperatures.

References

- 1 Ward, F. *Diamonds*. Gem, Bethesda, MD, 1998.
- 2 Field, J. E. *The Properties of Natural and Synthetic Diamond*. Academic Press, London, 1992.
- 3 Bundy, F. P. *J. Geophys. Res.*, 85 (1980), 6930.
- 4 Barnard, A. S. *The Diamond Formula - Diamond synthesis: a gemmological perspective*. Butterworth Heinemann, Oxford, 2000.
- 5 Charlier, J.-C., Gonze, X., and Michenaud, J.-P. *Europhys. Lett.*, 28 (1994), 403.
- 6 Hall, H. T. Ultrahigh-Pressure Research. *Science*, 128 (1958), 445-449.
- 7 Davies, G. *Diamond*. Adam Hilger, Bristol, 1984.
- 8 Eversole, W. G. *US Patent nos 3030187, 3030188*. 1958.
- 9 Angus, J. C., Will, H. C., and Stanko, W. S. *J. Appl. Phys.*, 39 (1968), 2915.
- 10 Matsumoto, S., Sato, Y., Tsutsumi, M., and Setaka, N. *J. Mater. Sci.*, 17 (1982), 3106.
- 11 Seal, M. *Diamond Relat. Mater.*, 1 (1992), 1075.
- 12 Anthony, T. R. and Banholzer, W. F. *Diamond Relat. Mater.*, 1 (1992), 717.

- 13 Liu, D., Sun, H., Pomeroy, J. W., Francis, D., Faili, F., Twitchen, D. J., and Kuball, M. *Appl. Phys. Lett.*, 107 (2015), 251902.
- 14 Nistor, P., May, P. W., Tamagnini, F., Randall, A., and Caldwell, M. *Biomaterials*, 61 (2015), 139.
- 15 Pillon, M., Angelone, M., and Krasilnikov, A. V. *Nucl. Instrum. Methods Phys. Res. B*, 101 (1995), 473.
- 16 Mainwood, A. *Semicond. Sci. Technol.*, 15 (2000), R55.
- 17 Watanabe, H., Koretsune, T., Nakashima, S., Saito, S., and Shikata, S. *Phys. Rev. B*, 88 (2013), 205420.
- 18 Wei, L., Kuo, P. K., Thomas, R. L., Anthony, T. R., and Banholzer, W. F. *Phys. Rev. Lett.*, 70 (1993), 3764.
- 19 Qui, W., Baker, P. A., Velisavljevic, N., Vohra, Y. K., and Weir, S. T. *J. Appl. Phys.*, 99 (2006), 064906.
- 20 Choy, K. L. *Prog. Mater. Sci.*, 48 (2003), 57.
- 21 May, P. W. Diamond thin films: a 21st-century material. *Phil. Trans. R. Soc. Lond. A*, 358 (2000), 473-495.
- 22 Ashfold, M. N. R., May, P. W., Rego, C. A., and Everitt, N. M. *Chem. Soc. Rev.*, 23 (1994), 21.
- 23 Element 6.
<http://www.e6.com/wps/wcm/connect/semiconwest/home/brochures/registration/brochure+download?BrochureLink=/wps/wcm/connect/semiconwest/home/brochures /brochure+download>, Accessed 05/09/17.
- 24 Dischler, B. and Wild, C. *Low-pressure synthetic diamond*. Springer, Berlin, Germany, 1998.
- 25 Ohtake, N. and Yoshikawa, M. *J. Electrochem. Soc.*, 137 (1990), 717.
- 26 Hanssen, L. M., Carrington, W. A., Butler, J. E., and Snail, K. A. *Mater. Lett.*, 7 (1988), 289.
- 27 Lieberman, M. and Lichtenberg, A. *Principles of plasma discharges and materials processing*. Wiley, New York, USA, 1994.
- 28 Roth, J. R., Rahel, J., Dai, X., and Sherman, D. M. *J. Phys. D: Appl. Phys.*, 38 (2005), 555.
- 29 Hartmann, P., Haubner, R., and Lux, B. *Diamond Relat. Mater.*, 5 (1996), 850.
- 30 Lee, W.-S., Baik, Y.-J., and Chae, K.-W. *Thin Solid Films*, 435 (2003), 89.
- 31 Wang, W., Liao, K., Gao, J., and Liu, A. *Thin Solid Films*, 215 (1992), 174.
- 32 Lee, W.-S., Chae, K.-W., Eun, K. Y., and Baik, Y.-J. *Diamond Relat. Mater.*, 10 (2001), 2220.
- 33 Chae, K.-W., Baik, Y.-J., Park, J.-K., and Lee, W.-S. *Diamond Relat. Mater.*, 19 (2010), 1168.
- 34 Sawabe, A., Yasuda, H., Inuzuka, T., and Suzuki, K. *Appl. Surf. Sci.*, 33 (1988), 539.

- 35 Stoner, B. R., Ma, G. H., Wolter, S. D., Glass, J. T., Zhu, W., Wang, Y.-C., and Davis, R. F. *Diamond Relat. Mater.*, 2 (1993), 142.
- 36 Badzian, A. R., Badzian, T., Roy, R., Messier, R., and Spear, K. E. *Mater. Res. Bull.*, 23 (1988), 531.
- 37 May, P. W. and Mankelevich, Y. *J. Phys. Chem. C*, 112 (2008), 12432.
- 38 Ohtake, N. and Yoshikawa, M. *J. Electrochem. Soc.*, 137 (1990), 717.
- 39 Sciortino, S., Lagomarsino, S., Pieralli, F., Borchi, E., and Galvanetto, E. *Diamond Relat. Mater.*, 11 (2002), 573.
- 40 Noda, M. *J. Indian Inst. Sci.*, 81 (2001), 627.
- 41 Metcalf, A., Fern, G. R., Hobson, D. R., Lefevre, G., and Saenger, R. *J. Instrum.*, 12 (2017), C01066.
- 42 Sigmund, P. *Particle Penetration and Radiation Effects. Springer Series in Solid State Sciences, 151.* Springer, Berlin, Germany, 2006.
- 43 Landau, L. *J. Phys. (USSR)*, 8 (1944), 201.
- 44 Kittel, C. *Introduction to Solid State Physics.* Wiley India Pvt Ltd, New Delhi, India, 2007.
- 45 Streetman, B. G. and Banerjee, S. *Solid State Electronic Devices.* Prentice Hall, New Jersey, USA, 2000.
- 46 Friedl, M. *Diamond Detectors for Ionizing Radiation.* Diploma thesis, University of Technology, Vienna, 1999.
- 47 Kania, D. R., Landstrass, M. I., Plano, M. A., Pan, L. S., and Han, S. *Diamond Relat. Mater.*, 2 (1993), 1012.
- 48 Sato, Y., Murakami, H., Shimaoka, T., Tsubota, M., and Kaneko, J. H. *Jpn. J. Appl. Phys.*, 55 (2016), 046401.
- 49 Adam, W. *et al.*, *Nucl. Instrum. Methods Phys. Res. A*, 565 (2006), 278.
- 50 Bauer, C. *et al.*, *Nucl. Instrum. Methods Phys. Res. A*, 367 (1995), 207.
- 51 Hassard, J. *Nucl. Instrum. Methods Phys. Res. A*, 368 (1995), 217.
- 52 Pillon, M., Angelone, M., Lattanzi, D., *et al.*, *Fusion Eng. Des.*, 82 (2007), 1174.
- 53 Angelone, M., Lattanzi, D., Pillon, M., *et al.*, *Nucl. Instrum. Methods Phys. Res. A*, 595 (2008), 616.
- 54 Lattanzi, D., Angelone, M., Pillon, M., *et al.*, *Fusion Eng. Des.*, 84 (2009), 1156.
- 55 Kopecky, J. *Atlas of Neutron Capture Cross Sections (IAEA INDC(NDS)-362).* IAEA, Vienna, Austria, 1997.

- 56 Unal, R. and Dean, E. B. Taguchi approach to design optimization for quality and cost: an overview. (New Orleans, USA 1991), Proceedings of the International Society of Parametric Analyst 13th Annual Conference.
- 57 Palubiski, D. R. *Pulsed Direct-Current Plasma Assisted Chemical Vapor Deposition (PDC PA-CVD); startup, optimization and its application in creation of isotopically pure diamond layers*. MSci thesis, University of Bristol, Bristol, UK, 2016.
- 58 Solel, T. *Analysing the Growth Characteristics of a Pulsed Direct Current Plasma Deposition Reactor (PDC PDR)*. MSci thesis, University of Bristol, Bristol, UK, 2017.
- 59 Advanced Energy. <http://www.advanced-energy.com/upload/file/dc/eng-pnclplus-210-05.pdf>, Accessed 05/09/17.
- 60 Swagelok. <https://www.swagelok.co.uk/en/product/Hoses-and-Flexible-Tubing/PFA-Flexible-Tubing>, Accessed 05/09/17.
- 61 Kurt J. Lesker. http://www.lesker.com/newweb/flanges/viewports_cf_glass.cfm?pgid=0, Accessed 04/09/17.
- 62 Bürkert. <https://www.burkert.co.uk/en/type/8715>, Accessed 05/09/17.
- 63 MKS. <https://www.mksinst.com/product/Category.aspx?CategoryID=72>, Accessed 05/09/17.
- 64 Edwards. <http://mmrc.caltech.edu/Vacuum/Edwards/%20RV%20Rotary%20Vane%20pumps/RV%20User%20Manual.pdf>, Accessed 05/09/17.
- 65 Spitsyn, B., Bouilov, L., and Derjaguin, B. *J. Cryst. Growth*, 52 (1981), 219.
- 66 Lee, H.-J., Jeon, H., and Lee, W.-S. *J. Appl. Phys.*, 109 (2011), 023303.
- 67 Suzuki, K., Sawabe, A., and Inuzuka, T. *Jpn. J. Appl. Phys.*, 29 (1990), 153.
- 68 Prawer, B. S. and Nemanich, R. J. *Phil. Trans. R. Soc. Lond.*, 362 (2004), 2537.
- 69 Hodkiewicz, J. *Characterizing Carbon Materials with Raman Spectroscopy*. Thermo Fisher Scientific, Madison, WI, USA, 2010.
- 70 Tuinstra, F. and Koenig, J. L. *J. Chem. Phys.*, 53 (1970), 1126.
- 71 Wanlu, W., Kejun, L., Jinying, G., and Aimin, L. *Thin Solid Films*, 215 (1992), 174.
- 72 Dismukes, J. P. *Proceedings of the Third International Symposium on Diamond Materials*. The Electrochemical Society, Pennington, USA, 1993.
- 73 Ecker, G. and Emeleus, K. G. *Ann. Phys.*, 470 (1965), 53.

Certification of ownership of the copyright in a typescript or manuscript

Dissertation presented as part of, and in accordance with, the requirements for the Final Degree of MSc in Nuclear Science and Engineering at the University of Bristol, Faculty of Science.

I hereby assert that I own exclusive copyright in the item named below. I give permission to the University of Bristol Library to add this item to its stock and to make it available for consultation in the library, and for inter-library lending for use in another library. It may be copied in full or in part for any *bona fide* library or research worked, on the understanding that users are made aware of their obligations under copyright legislation, *i.e.* that no quotation and no information derived from it may be published without the author's prior consent.

Author	Edmund Smith
Title	Optimization of Pulsed Direct Current Plasma-Assisted Chemical Vapour Deposition (PDC PA-CVD) and its Use to Create Isotopically Pure Diamond for Radiation Detection Applications
Date of Submission	07/09/2017

Signed: E. Smith

Full name: Edmund Jack William Smith

Date: 07/09/2017

This project/dissertation is the property of the University of Bristol Library and may only be used with due regard to the rights of the author. Bibliographical references may be noted, but no part may be copied for use or quotation in any published work without the prior permission of the author. In addition, due acknowledgement for any use must be made.